NAVAL POSTGRADUATE SCHOOL

MONTEREY, CALIFORNIA

THESIS

EVALUATION OF HIGH DENSITY SURFACE OBSERVATIONS IN COMPLEX TERRAIN AND THEIR CONTRIBUTION TO THE MM5 MODEL

by

Paul B. Homan

March 2007

Thesis Advisor:	Wendell A. Nuss
Second Reader:	Karl D. Pfeiffer

Approved for public release; distribution is unlimited

THIS PAGE INTENTIONALLY LEFT BLANK

REPORT DOCUMENTATION PAGE		*Form Approved OMB No. 0704-0188*

Public reporting burden for this collection of information is estimated to average 1 hour per response, including the time for reviewing instruction, searching existing data sources, gathering and maintaining the data needed, and completing and reviewing the collection of information. Send comments regarding this burden estimate or any other aspect of this collection of information, including suggestions for reducing this burden, to Washington headquarters Services, Directorate for Information Operations and Reports, 1215 Jefferson Davis Highway, Suite 1204, Arlington, VA 22202-4302, and to the Office of Management and Budget, Paperwork Reduction Project (0704-0188) Washington DC 20503.

1. AGENCY USE ONLY *(Leave blank)*	2. REPORT DATE March 2007	3. REPORT TYPE AND DATES COVERED Master's Thesis	
4. TITLE AND Subtitle Evaluation of High Density Surface Observations in Complex Terrain and their Contribution to the Mm5 Model		5. FUNDING NUMBERS	
6. AUTHOR(S) Paul B Homan			

7. PERFORMING ORGANIZATION NAME(S) AND ADDRESS(ES)
   Naval Postgraduate School
   Monterey, CA 93943-5000
		8. PERFORMING ORGANIZATION REPORT NUMBER	

9. SPONSORING /MONITORING AGENCY NAME(S) AND ADDRESS(ES) N/A		10. SPONSORING/MONITORING AGENCY REPORT NUMBER	

11. SUPPLEMENTARY NOTES The views expressed in this thesis are those of the author and do not reflect the official policy or position of the Department of Defense or the U.S. Government.

12a. DISTRIBUTION / AVAILABILITY STATEMENT Approved for public release; distribution is unlimited	12b. DISTRIBUTION CODE

13. ABSTRACT (maximum 200 words)

This study evaluates the data assimilation capabilities of Three Dimensional Multiquadric Interpolation (3DMQ) and the MM5 model when incorporating mesoscale observations from the United States Air Force Academy (USAFA) High Wind Alert system (HWAS). These mesoscale observations are incorporated into a triple nested (12, 4, and 1.33 km) high resolution model simulation and evaluated for their impact upon analyzed and forecasted wind values at USAFA during a severe downslope wind event that occurred on 6 March 2004. This evaluation is the first step in developing future forecasting and analysis tools for use by the military in various operations in complex terrain. The development of deployable automated tactical weather sensors in forward deployed locations requires an evaluation of the impact and usefulness these sensors would have on analysis forecast tools and mesoscale Numerical Weather Prediction (NWP) models. The juxtaposition of the HWAS network in complex terrain and the aviation training operations at USAFA provides an ideal set of data, mission and location for testing and evaluating a high resolution nested grid mesoscale NWP model. This study shows that incorporating HWAS observations into the 3DMQ data assimilation process has a significant impact upon verification of analyzed wind fields with the biggest impact occurring at the 1.33 km grid scale. Using these analyzed fields as initial conditions for MM5 model simulations, this study shows the ability of the 1.33 km model forecast wind fields to verify significantly better than either the 4 or 12 km through 18, 24, and 30 hour forecasts. Additionally, this study shows the limited, yet discernable impact HWAS observations have upon forecasted winds in the first several hours of MM5 model runs during a severe downslope wind event at USAFA.

14. SUBJECT TERMS Mesoscale Observations, Complex Terrain, High Resolution Model, Tactical Weather Observations, Numerical Weather Prediction, MM5, Three Dimensional Multiquadric Interpolation, Downslope Wind, Chinook, Bora, Data Assimilation, Initial Conditions, Nested Grid Model, Mountains			15. NUMBER OF PAGES 95
			16. PRICE CODE
17. SECURITY CLASSIFICATION OF REPORT Unclassified	18. SECURITY CLASSIFICATION OF THIS PAGE Unclassified	19. SECURITY CLASSIFICATION OF ABSTRACT Unclassified	20. LIMITATION OF ABSTRACT UL

NSN 7540-01-280-5500

Standard Form 298 (Rev. 2-89)
Prescribed by ANSI Std. 239-18

THIS PAGE INTENTIONALLY LEFT BLANK

EVALUATION OF HIGH DENSITY SURFACE OBSERVATIONS IN COMPLEX TERRAIN AND THEIR CONTRIBUTION TO THE MM5 MODEL

Paul B. Homan
Captain, United States Air Force
B.S., United States Air Force Academy, 2002

Submitted in partial fulfillment of the
requirements for the degree of

MASTER OF SCIENCE IN METEOROLOGY

from the

NAVAL POSTGRADUATE SCHOOL
March 2007

Author: Paul B. Homan

Approved by: Wendell A. Nuss
               Thesis Advisor

               Karl D. Pfeiffer
               Second Reader

               Phillip A. Durkee
               Chairman, Department of Meteorology

THIS PAGE INTENTIONALLY LEFT BLANK

ABSTRACT

This study evaluates the data assimilation capabilities of Three Dimensional Multiquadric Interpolation (3DMQ) and the MM5 model when incorporating mesoscale observations from the United States Air Force Academy (USAFA) High Wind Alert system (HWAS). These mesoscale observations are incorporated into a triple nested (12, 4, and 1.33 km) high resolution model simulation and evaluated for their impact upon analyzed and forecasted wind values at USAFA during a severe downslope wind event that occurred on 6 March 2004. This evaluation is the first step in developing future forecasting and analysis tools for use by the military in various operations in complex terrain. The development of deployable automated tactical weather sensors in forward deployed locations requires an evaluation of the impact and usefulness these sensors would have on analysis forecast tools and mesoscale Numerical Weather Prediction (NWP) models. The juxtaposition of the HWAS network in complex terrain and the aviation training operations at USAFA provides an ideal set of data, mission and location for testing and evaluating a high resolution nested grid mesoscale NWP model. This study shows that incorporating HWAS observations into the 3DMQ data assimilation process has a significant impact upon verification of analyzed wind fields with the biggest impact occurring at the 1.33 km grid scale. Using these analyzed fields as initial conditions for MM5 model simulations, this study shows the ability of the 1.33 km model forecast wind fields to verify significantly better than either the 4 or 12 km through 18, 24, and 30 hour forecasts. Additionally, this study shows the limited, yet discernable impact HWAS observations have upon forecasted winds in the first several hours of MM5 model runs during a severe downslope wind event at USAFA.

THIS PAGE INTENTIONALLY LEFT BLANK

TABLE OF CONTENTS

LIST OF FIGURES

LIST OF TABLES

THIS PAGE INTENTIONALLY LEFT BLANK

ACKNOWLEDGMENTS

THIS PAGE INTENTIONALYY LEFT BLANK

I.   INTRODUCTION

A.   MOTIVATION

In the United States Military, current engagements at the operational and tactical levels are increasingly dependent upon weather forecast accuracy. This requirement is also coupled with a demand for increased forecast resolution while retaining accuracy. The age of modern warfare with precision engagement is aided by Laser Guided Bombs, Global Positioning Satellites, infrared and microwave imaging, etc. that often require accurate weather forecasts on the order of 1-2 km resolution or even less. Current operational global numerical weather prediction (NWP) models such as the GFS and NOGAPS have resolutions on the order of 40-60 km, while mesoscale models such as the WRF, COAMPS, and MM5 generally run at 45-54 km with resolutions of 12-15 km over some regions.

Recent advancements in computing technology together with increased linking and density of available data from observational networks have given rise to the possibility of NWP models that have meaningful forecast information with resolutions on the order of 1-2 km (Mass et al. 2002). In 2004, a meso-net of 12 automated meteorological observing stations was placed in various locations along the Front Range of the Rocky Mountains in and around the United States Air Force Academy (USAFA). This network was aptly named the High Wind Alert System (HWAS) after the strong winds that often frequent this region.   A continuous set of HWAS data extends back to 1 Feb 2004. The spatial/temporal resolution of HWAS data offers a unique opportunity to quantify and reveal important mesoscale boundary layer phenomena for use by local forecasters. Additionally, future high resolution mesoscale models (WRF, etc.) will operate in regions with complex terrain and forward-deployed tactical weather sensors will provide limited battlespace observations. The HWAS network also offers an opportunity to assess the impact of improved mesoscale data assimilation using a few targeted HWAS observations.

B.   PROBLEM STATEMENT

The Air Force Weather Agency (AFWA) has requested the documentation of model performance in complex terrain that could lead to the future development of forecasting and analysis tools for use by the military in various operations in complex terrain.   Additionally, the development of deployable automated tactical weather sensors in forward deployed locations requires an evaluation of the impact and usefulness these sensors would have on analysis forecast tools and mesoscale NWP models.   The juxtaposition of the HWAS network in complex terrain and the aviation training operations at USAFA provides an ideal set of data, mission and location for testing and evaluating a high resolution nested grid mesoscale NWP model that assimilates mesoscale observations into its data analysis.   Not only would such a model aid weather forecasters in support of USAFA operations, but serve as an example that could be duplicated and used in support of a variety of military operations in regions of mountainous terrain.

Perhaps the most volatile forecasted meteorological variable in complex terrain is the wind.   Dramatic differences in observed wind intensity can occur over very short spatial and temporal scales.   Winds at USAFA are often the most disruptive meteorological variable to USAFA operations and therefore are the parameter that will be given the most consideration in this study.   Although the HWAS network does a good job at monitoring winds at USAFA in real-time, operational forecast models do a very poor job due to their limited representation of terrain and poor grid resolution.   Incorporating high resolution terrain information and the mesoscale HWAS observations into a model that has more spatial and temporal resolution than current operational models, should aid the ability to forecast strong wind events at USAFA more accurately and demonstrate the impact and need for mesoscale observations in tactical NWP applications.   However, the insertion of mesoscale observations into a high resolution model could potentially produce more noise than signal as not all mesoscale features in each domain would be appropriately resolved.   This could

2

impact the ability of the model to accurately predict small scale structures and adversely affect forecast accuracy.

C.   RESEARCH OBJECTIVES

The meteorological and climatological studies that can be derived from a rich data set such as the HWAS network are almost innumerable. Although the HWAS data set is a rich source for in-depth, boundary layer, mesoscale meteorology, and climatology studies, the general goal and focus of this research is to find optimum ways to represent and incorporate this data into analysis and forecast tools that may be used as an example to pave the way for higher resolution and more accurate forecasting tools that will be used to impact operational planning and execution of military operations. Finding ways to optimally incorporate the HWAS data into analysis schemes and mesoscale weather models will also help future studies that take a more in-depth look at mesoscale weather and climatological phenomena in this region. It is an aim of this research to determine how important assimilating observations into a high resolution NWP model might be in complex terrain and to what extent assimilating these observations would help or hinder forecast accuracy.

The specific goals of this research are to:

1. Apply and evaluate an interpolation scheme that incorporates HWAS observations into a mesoscale analysis using mesoscale first guess fields.

2. Evaluate and quantify the impact of HWAS observations on the mesoscale analysis in complex terrain.

3. Apply a nested grid structured NWP model that incorporates HWAS and other observations in its model runs and output fields for the USAFA region.

4. Investigate the impacts of incorporating HWAS observations into a nested grid structured NWP model on the predictability of wind values on the 1-4 km scale in complex terrain.

II. BACKGROUND

Since the development of the first NWP model, there has always been a demand for models with higher resolution. It was expected that models with higher resolution would produce a more accurate higher fidelity forecast than models with coarser resolution. The idea of tailoring the weather forecast for a specific location became very popular especially when applied to military planning and operations. Unlike most civilian sector weather applications that are often fixed at a certain location, the nature of modern military operations with a rapidly changing battlefield aided by modern aircraft and weaponry are begging for more accurate and more detailed weather forecasts. However, the accuracy of high resolution NWP models in complex terrain, the need for and ability to assimilate limited mesoscale observations into these models, as well as the fundamental limits on predictability are not well known.

A. OVERVIEW-- NUMERICAL FORECAST MODELS

In the first few decades of model development, numerous NWP models and forecast techniques were developed and tested that helped lead to the development of today's current operational models. This section summarizes the predominant early operational models that were developed at the National Meteorological Center (NMC) that later became the National Centers for Environmental Prediction (NCEP). The operational NWP models that exist today are discussed in subsequent sections.

1. History of NWP Models- Resolution

Increasing the resolution of NWP models has always been linked with the current available computer power and technology. In the 1950's a single level barotropic model that covered North America and adjacent waters was developed by the NMC. This barotropic model was run on an IBM 701 with a 30 X 34 grid and a grid resolution of 381 km. In 1966, a more robust six layer

primitive equation model became operational due to the much faster computational speed of the CDC 6600. This coincided with the appearance of the U.S. Air Force Automated Weather Network which allowed initial data to be collected more rapidly and thus start the operation of the model earlier. This six layer primitive equation model was run on a larger 53 X 57 grid, but still with a resolution of 381 km. In 1971, the Limited-Area Fine-Mesh (LFM) was introduced as the first regional operational model. It was very similar to the six layer primitive equation model, but was run at half the mesh size, half the time step, and a smaller area. The LFM's resolution was initially 190.5 km and was reduced to 127 km in 1977. However, its resolution was increased back to 190.5 km in 1981 with the introduction of fourth order difference systems. The LFM covered an octant of the globe having 53 X 45 grid points on the smaller interval and 79 X 67 on the larger (Shuman 1989).

The first global model was introduced in 1974 when a finite difference model was established with a grid interval of 2.5 lat-long degrees and nine layers. The Global Spectral Model replaced the nine layer model in 1980 with a resolution of 12 layers in the vertical and 30 spherical harmonic modes in the horizontal (T30L12). To save computer time, at 48 hours its horizontal resolution was decreased to 24 modes, at 144 hours its vertical resolution was decreased to six layers, and at eight days its number of modes was halved by reducing the effective area of prediction to the Northern Hemisphere (Shuman 1989).

2.   Current Operational Models- Resolution

Today there is a plethora of NWP models from many different countries and organizations all over the world that are readily available to a forecaster. This section will only summarize a few of the primary operational NWP models readily available for use by the military forecaster, primarily focusing on the continued progression of models with ever increasing detail and resolution.

The ETA model is a regional mesoscale model run by NCEP over North America that uses enhanced terrain and improved parameterization of surface and precipitation processes (NCEP Product Document Description, 2004). It was selected to replace the NGM model at NCEP in June 1993. Originally its operational forecasts were run to 48 hours twice daily, starting from 00 UTC and 12 UTC using 80 km horizontal resolution and 38 vertical levels. Initial analyses were based on Optimum Interpolation (OI) using a first guess from the Global Data Assimilation System (GDAS). Subsequent improvements allowed it to be run at 48 km resolution in October 1995, 32 km with 45 vertical levels in February 1998, 22 km with 50 vertical layers in September 2000, to its current operational resolution of 12 km and 60 vertical layers run four times a day in November 2001. The ETA model took on the new name of the North American Mesoscale (NAM) model in January 2005 with no model change at that time (UCAR ETA Introduction, 2005). On June 20, 2006, NCEP replaced the ETA model and its ETA 3d-var analysis running in the NAM slot with the NCEP Nonhydrostatic Mesoscale Model (NMM) and Gridpoint Statistical Interpolation (GSI) analysis running in the Weather Research and Forecasting (WRF) infrastructure. All NAM output is now from the WRF-NMM rather than from the ETA model. The domain, horizontal resolution, and output grid geometry did not change (UCAR NAM Model Changes, 2006).

The MM5 (Mesoscale Model, Version 5) is the Air Force's fine-scale meteorological model of choice. The Air Force Weather Agency (AFWA) declared MM5 operational on 28 October 1997. The MM5 is the fifth-generation mesoscale model developed by the National Center for Atmospheric Research (NCAR) and The Pennsylvania State University. The original version was built in the 1970s and has undergone improvements to evolve into the MM5 used today. Currently, AFWA's operational runs are done in a nested grid with 45 and 15 km horizontal resolution and 42 levels of vertical resolution. In some regions of interest, the AFWA MM5 is run at and produces forecast products with a 5 km horizontal grid resolution (UCAR Operational Models Matrix, 2007). AFWA is also currently running the WRF model in an experimental mode with the same

grid resolutions as their current MM5 model and plans to use a version of the WRF model operationally in the near future (Cunningham 2007).

The Global Forecast System (GFS) is one of only a couple of global spectral models that are currently operational. The GFS is currently run and maintained by NCEP and grew out of the Global Spectral Model described in the previous section. Major changes were made to the Global Spectral Model in 1985 at which point it was renamed the Medium Range Forecast (MRF) model. These changes included new physics packages, an increase in the number of waves resolved to rhomboidal truncation at 40 waves (R40), and an increase in the number of equally spaced layers from 12 to 18. Currently, the GFS is run four times per day (00, 06, 12, and 18 UTC) out to 384 hours. The initial forecast resolution was changed on May 31, 2005 to T382L64 (equivalent to about 40 km grid-point resolution) with 64 levels out to 7.5 days (180 hours). At later forecast times, the GFS has a resolution of T190L64 (equivalent to about 80 km resolution) and 64 levels beyond to day 16 (384 hours). All GFS runs get their initial conditions from the Spectral Statistical Interpolation (SSI) global data assimilation system (GDAS), which is updated continuously throughout the day (UCAR GFS Introduction, 2005).

The Navy Operational Global Atmospheric Prediction System (NOGAPS) is a global model that is spectral in the horizontal and energy-conserving finite difference (sigma coordinate) in the vertical. NOGAPS is run and maintained at the U.S. Navy's Fleet Numerical Meteorology and Oceanography Center (FNMOC). In September 2002, NOGAPS 4.0 was increased in resolution from T159L24 to T239L30, an increase in equivalent grid point resolution from about 0.75 to 0.5 degrees or about 55 km in the tropics (UCAR Operational Models Matrix, 2007).

B. FORECAST ACCURACY AND PREDICTIBILITY IN COMPLEX TERRAIN

Mesoscale NWP in areas of complex terrain is often difficult. For example, over the Intermountain West, forecast skill lags other regions of the country due to upstream data-void regions, limitations associated with the use of in situ and remotely sensed data over complex terrain, and weaknesses in conceptual models of airflow interaction with topography (Schultz et al. 2002). Other difficulties have arisen such as the sensitivity of rainfall patterns to errors in the large-scale ambient wind, validating nonuniform precipitation patterns, the simulation of cold pools in valleys and basins, and the collective and multiscale effects of complex terrain (Smith et al. 1997). The term "predictability" refers to the potential to produce forecasts in which the signal exceeds the noise due to the uncertainty of the forecast system. In meteorology, predictability connotes a somewhat narrower meaning, related solely to the time evolution of uncertainties associated with the specifications of the initial state (Paegle et al. 1990).

The investigation of dynamical systems in the 1960s and 1970s resulted in the development of the concept of chaos (Lorenz 1963). The idea of chaos has been used to define the limits of predictability of weather forecasts. One of the characteristics of a chaotic regime is a sensitivity to initial conditions such that infinitesimal differences in initial conditions will result in solutions at a later time that are uncorrelated with one another. As many other systems in weather such as convective systems and even quasi-geostrophic flow have shown a chaotic behavior, it is reasonable to assume that mesoscale atmospheric flow may exhibit chaos or finite predictability (Paegle et al. 1990). For complex terrain, the ability to represent the terrain and the initial mass and momentum fields is challenging. However, the assimilation of mesoscale observations, such as the HWAS network, and high resolution terrain information into analysis and first guess fields may give rise to the capability to improve the predictive ability of NWP models at scales previously thought too chaotic for a model to resolve.

9

In a paper assessing processes responsible for the Great Salt Lake-effect snowstorm of 7 December 1998, Onton and Steenburgh (2001) used a series of mesoscale model simulations to examine issues related to predictability by present-day numerical models. Their simulations modified lake-surface temperature and upstream moisture to illustrate how small errors in the specification of these quantities can impact quantitative precipitation forecasts and potentially limit the utility of high resolution mesoscale model guidance. Ultimately, they asserted that it is possible that the intense local forcing of the Great Salt Lake and surrounding topography may simply exacerbate large-scale model errors, and limit the utility of mesoscale numerical model forecasts, but they conceded that much more research examining the predictive ability of mesoscale models is needed.

One idea proposed concerning the predictability of forecast variables in complex terrain is that strongly forced and highly dissipated local slope circulations may be inherently more predictable than flows over flat terrain that are more sensitive to initial data errors (Paegle et al. 1990). The effect of initial and boundary conditions on the ability of a mesoscale model to predict jet maxima on the flanks of the Alps was studied by Paegle and Vukicevic (1987). Using a detailed boundary-layer forecast model initialized from smooth operational analyses of the ECMWF (European Centre for Medium Range Weather Forecasts), they concluded that the predicted location of low-level jets and circulation maxima are relatively insensitive to both random and systematic analysis differences of initial data. They concluded that the model's ability to predict jet maxima on the flanks of the Alps, even though the jet maxima is missing in the smoothed initial and boundary conditions provided by the ECMWF analyses suggests that the boundary effects of topography improve the predictability of low-level flows in ways that are unrelated to the initial and boundary condition specification (Paegle et al. 1990). Other studies have also given examples of fine-scale forecasts emerging from smooth initial and boundary data including Paegle et al. (1984) and Astling et al. (1985).

10

Predictability experiments with limited area domains and nested sequences of models have also yielded unique results for forecast models in complex terrain. One such experiment by Berri and Paegle (1989) analyzed signal/noise ratios of a model simulation over the highly mountainous terrain of the Andes. Their conclusion was that the signal/noise ration was on the order of 4 to 1 and that the steep topography amplified the low-level signal sufficiently to make a deterministic forecast feasible. Due to the spreading of lateral boundary errors toward the center of a limited area domain, sensitivity studies of regional models (Paegle and Vukicevic 1987; Vukicevic and Paegle 1989) suggest that accurate lateral boundary conditions may be the most important single ingredient for an accurate local forecast. Paegle et al. (1990) summarizes a series of experiments dealing with lateral boundary error. They conclude that the results offer hope for accurate local prediction in a nested sequence of models provided the coarse domain forecasts contain accurate boundary information on scales that are comparable to the larger scale structures resolved by the more finely resolved nested subdomain. They also suggest that boundary information on scales much smaller than the perimeter of the boundary may not be especially relevant near the center of the forecast domain. This conclusion was based on and entirely consistent for purely diagnostic models. Its applicability to complete forecast models remains uncertain.

C. RECENT STUDIES OF INCREASED RESOLUTION IN COMPLEX TERRAIN

There have been numerous simulations and NWP model studies in the past 10 years that have increased model resolution below 10 km and into the single digits. Overall, increasing resolution has provided better defined and more realistic structures when evaluated subjectively. However, only a few studies have shown that forecast accuracy when measured objectively over an extended period of time increases as grid spacing decreases below approximately 10-15 km (Mass et al. 2002). This section reviews several of these studies that were conducted in areas of complex terrain.

As summarized in Mass et al. (2002) both subjective and objective evaluations have found clear benefits of increasing resolution in areas where orographic flows or diurnal circulations are present. Using the Colorado State RAMS model with a max resolution of 2.5 km for 12 hour predictions in the Susquehanna River Valley of Pennsylvania, McQueen et al. (1995) found that the 2.5 km grid in combination with high vertical resolution produced far more realistic structures than predicted in the 10 km domain. This experiment assimilated two local wind observations into all grid domains and analyzed the appropriate nudging weight of each of these observations and their effect on the output wind fields. The best nudging weighting value for these observations was found to be 0.002 and they concluded that assimilation had only a small but positive effect on the forecast winds when using the appropriate weighting function. This positive effect was not limited to areas close to the observations, but also to other areas within the valley as wind predictions were aided by assimilation indirectly including topographical forcing that was not fully accounted for without nudging.

Colle and Mass (1998) using stationary 9, 3, and 1 km domains nested within a 27 km domain used the MM5 to evaluate a severe downslope windstorm on the western side of the Cascades. They used 31 unevenly spaced vertical sigma levels with maximum resolution in the boundary layer. Five-minute averaged terrain data were analyzed to the 27 and 9 km model grids using a Cressman analysis scheme. For the 3 km and 1 km domains, a 30 second topography dataset was interpolated to the grid in order to better resolve the Olympic and Cascade Mountains. Initial conditions were generated for the 27 and 9 km domains by interpolating the NCEP global analyses (2.5 degrees latitude–longitude resolution) to the model grid. These analyses were improved by incorporating surface and upper-air observations using a Cressman-type analysis scheme. Additional analyses generated in the same manner every 12 hours were linearly interpolated in time in order to provide the lateral boundary conditions for the 27 km domain. They concluded that the 1 km MM5 simulation realistically simulated the downslope windstorm including the cold air damming

east of the Cascades, strong winds downstream of mountain gaps, and a mountain wake downstream of Mount Rainier.

A more objective evaluation of forecast accuracy in a 4 km domain nested within a 12 and 36 km domain using the MM5 over the Pacific Northwest over a period of several years is described in Mass et al. (2002). In this evaluation done at the University of Washington, initial and boundary conditions for the real time forecasts were obtained from the NCEP ETA model initial conditions and forecast fields. The model verification scheme made use of several regional observation networks that resulted in about 150 observations not included in the initial state within the 4 km domain covering the western half of Washington.

This study showed clear improvements in precipitation, 10m wind, 2m temperature, and sea level pressure forecasts as grid resolution increased from 36 to 12 km. However, no forecast variables performed better when verified objectively as the resolution was increased from 12 to 4 km. This decrease in skill score within the 4 km grid was attributed to timing or positional errors of the mesoscale feature. The results from this evaluation suggested that the model performance improved in mesoscale structures as the grid resolution increased from 36 to 12 km and increasing resolution from 12 to 4 km produced finer scale improvements by increasing the definition and intensity of mesoscale features when verified subjectively. They showed that subjective comparisons of observed and forecast structures suggest the value of increased resolution; however, objective evaluations using point verification and traditional skill scores such as absolute or root mean square errors result in somewhat different conclusions. Their inability to show objective improved forecast accuracy at their lowest resolution may have been influenced by the fact that they did not incorporate mesoscale observations into their data assimilation process.

Perhaps the most extensive objective verification of an increased resolution grid was done by Hart et al. (2005). Their forecast verification was conducted from 23 January to 25 March 2002 over a region that encompassed northern Utah. They incorporated observational data from MesoWest, a

collection of cooperative networks that includes surface weather observations from more than 180 providers and 6000 stations nationally with an emphasis on the Western United States. Model forecasts were provided by a real-time multi-nested 36, 12, and 4 km domain version of the MM5 that was run four times daily at the University of Utah for weather prediction during the Olympic and Paralympic Winter Games. Twenty-Seven half-sigma levels were used in the vertical with a higher concentration in the boundary layer. Observed terrain data, 10 minute resolution for the 36 km domain and 30 second resolution for the 12 and 4 km domain, were bilinearly interpolated to the MM5 grid. Initial and lateral boundary conditions were provided by the NCEP ETA model, with the Advanced Regional Prediction System (ARPS) Data Analysis System (ADAS) used to incorporate MesoWest surface observations into the near surface analysis.

The verification concentrated on northern Utah, an area roughly encompassed by the 4 km domain, a region that included all of the outdoor venues for the 2002 Olympic and Paralympic Games. This study concluded that increasing grid resolution from 12 to 4 km improved wind and precipitation forecasts over the fine-scale topography of the Intermountain West. These results are in contrast to previous studies that revealed no objective improvements at the highest resolution, but only subjective improvements. Hart et al. (2005) point out that the topographic differences in the half widths of the Intermountain West and the Pacific Ranges (Cascade Mountains, Olympic Mountains, and Sierra Nevada) with the Intermountain West having smaller half widths (~5 km) when compared to the Pacific Ranges (~50 km). They suggest that grid spacing smaller than 10 km is needed to begin to define the Intermountain West and the primary influences on local meteorology.

D.   RESEARCH FOCUS

Previous studies indicate that an in-depth analysis on the impacts to a model by the assimilation of mesoscale observations is needed. A better understanding between the relationship of lateral and boundary error and the impact of the observations on this error and the inherent signal-to-noise ratio

within a model simulation is needed. It is still unclear whether or not adding mesoscale observations would add to the signal of mesoscale features or distort them and instead add noise. Also, if the assimilation of the mesoscale observations does not decrease the lateral boundary error, would a more finely resolved analysis in the smallest subdomain demonstrate measurable improvement to a model run? If this is true, how long before lateral and boundary error would propagate to the center of the domain and dominate the forecast accuracy of the model?

Mesoscale data assimilation is still in its infancy and is not yet mature as many different methods and techniques to assimilate the wide variety of observations currently available still need to be investigated. New advancements in data analysis techniques have recently come to light with the application of multiquadric interpolation schemes for meteorological objective analysis (Nuss and Titley 1993). The method of multiquadric interpolation which uses hyperboloid radial basis functions to fit scattered data to a uniform grid has been shown to be more accurate for meteorological analysis than Barnes or Cressman methods. Applications to meteorological data show that multiquadric interpolation is able to produce analyses that retain small-scale features resolved by the observations in any subregion of the analysis. The ability of the multiquadric approach to retain small-scale structure has potential large implications if exploited for grids on the order of 1 km as operational 3DVAR systems are not currently ready or capable of assimilating data optimally on this scale with limited observations.

There is a great need in the military to assess the potential for inserting tactical observations into high resolution battlespace NWP models. As the technology and delivery platforms for these automated forward deployed systems are developed, an important cost analysis process will need to occur. Tactical observations come at a substantial cost in time and personnel. A better understanding of the usefulness of these observations in better characterizing the battlespace, and understanding these observations impact on numerical forecasts in complex terrain is paramount. The research conducted in this

experiment will ultimately examine the potential for tactical observations to be inserted into a mesoscale model using the multiquadric approach.

III. DATA AND METHODOLOGY

Strong downslope wind events at USAFA were selected for use in this study as they have a strong signal that frequently occurs and is well observed by the HWAS network. The highly intricate temporal and spatial structure of these wind events influenced by the complex terrain make them an ideal case study for this experiment. These wind events pose significant threats to the day to day operations of military training and flying activities at USAFA more so than any other weather phenomena. It was for this reason the HWAS network was envisioned and ultimately put in place. In addition, downslope winds such as those observed at USAFA are commonplace in many of the mountainous regions of the world where military operations are occurring or likely to occur in the future. A strong downslope wind event at USAFA was recorded by HWAS sensors on 6 March 2004 and was selected for use in this study. This downslope wind storm produced the highest gust recorded at any of the HWAS sensors in 2004 with a gust of 38 m/s at the Rampart sensor. However, this was not the only strong event in 2004 recorded by the HWAS network as there were several other downslope wind events that rivaled the 6 March 2004 event in intensity that would be ideal for research in future studies.

A. REGIONAL SUMMARY

1. Area Geography

USAFA lies at the base of the eastern slopes of the Front Range of the Rocky Mountains approximately 20 km northwest of Colorado Springs, Colorado. The Continental Divide runs north to south through Colorado and is 110 km to the northwest of USAFA and 135 km directly to the west (Figure 1). The average ridgeline elevation along the Continental Divide is 3600 m with several peaks greater than 4200 m. Although not entirely part of the Continental Divide, the Mosquito Range lies about 105 km to the west-northwest of USAFA with ridgelines of just over 3600 m and several peaks above 4200 m. The Tarryall

and Kenosha Mountains lie even closer at 70-80 km to the northwest with several peaks in the 3600 to 3800 m range.

The local dominant feature around USAFA is the Rampart Range. It runs north to south along the western flank of USAFA and the surrounding areas. Pikes Peak (4300 m) is the dominant feature of the Rampart Range and is located approximately 21 km southwest of the USAFA Airfield. The average ridgeline of the Rampart Range directly adjacent to USAFA is about 2700 m with several peaks around 2900 m.

The USAFA Reservation is 18,500 acres and varies greatly in elevation both north to south and east to west. There are several ridges that extend west to east from the Rampart Range along USAFA, with their average elevations ranging from 2225 to 2000 m. Between these ridges are valleys that range in elevation from 2050 to 1950 m. The main cadet area (often referred to as the Terrazzo) where the dormitories and academic buildings are located is positioned on one of these ridges at 2212 m. The USAFA Airfield lies at the mouth of Pine and Douglas Valleys with elevations ranging from 1990 to 2005 m. Jack's Valley, the main summertime training area lies on the north end of the USAFA Reservation and ranges in elevation from 2130 m to the west and 1980 m to the east. Monument Creek flows north to south along the eastern edge of USAFA and parallels Interstate 25 (I-25) and a set of railroad tracks from the northern boundary of USAFA to roughly where I-25 is adjacent to the stadium. At this point the creek and railroad tracks turn in a southwesterly direction and are west of the USAFA Airfield where the creek turns again roughly south and exits the USAFA Reservation just southwest of the South Gate. Monument Creek is the center of a valley that runs north to south with elevations increasing to the west and also to the east.
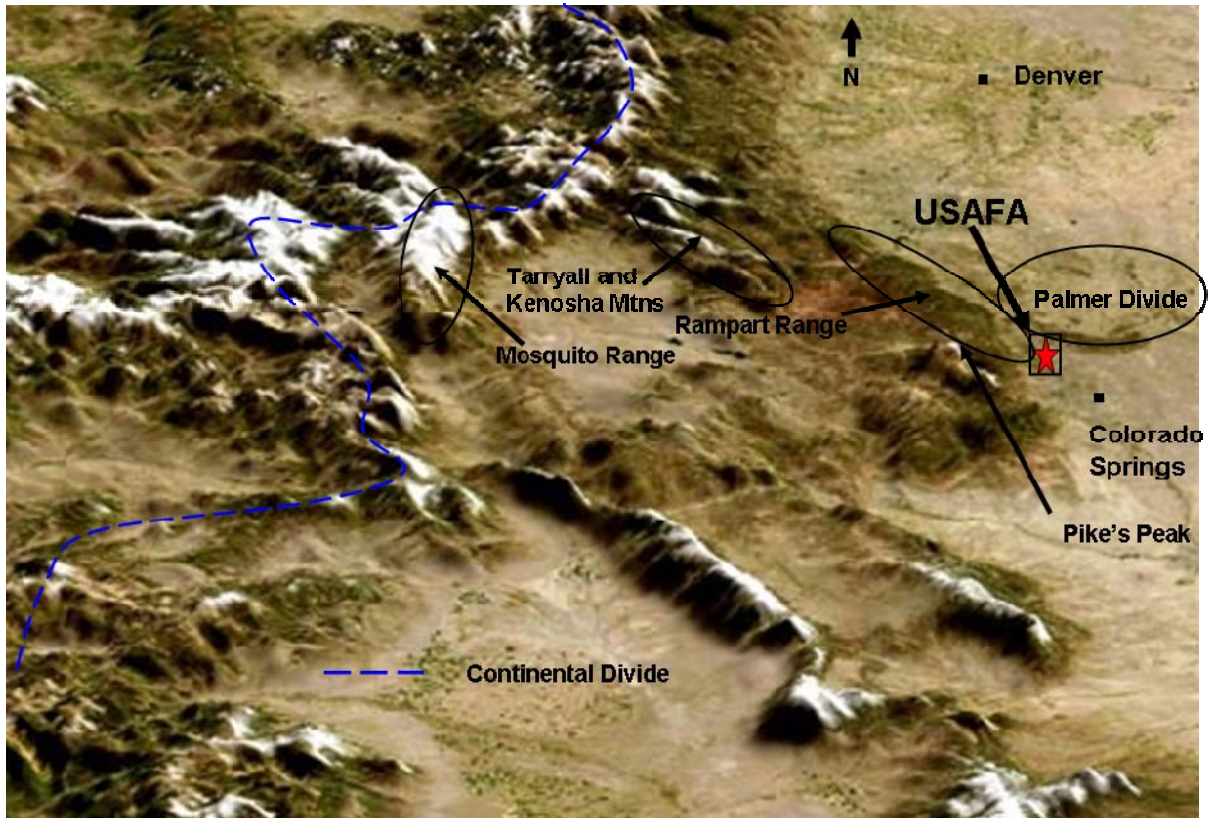
Figure 1.   Image showing mountain ranges in Colorado taken after first
snowfall in 2002. (After Descloitres, 2002).

Located about 18 km north of the USAFA Airfield and 13 km north of the cadet area is the crest of the Palmer/Monument Divide (sometimes referred to as the Palmer/Monument Ridge). This ridge extends east from the Rampart Range with an average elevation of 2280 m and maximum elevation above 2400 m. This ridge is the main geographical feature between Colorado Springs and Denver and measures north to south on average 45-55 km and runs from the Rampart Range 45-55 km east out onto the adjacent plains. Due to the Palmer Divide, elevations increase as you head north from USAFA as well as to the east. The region directly 6-12 km to the east of USAFA on the Palmer Divide is known as the Black Forest due to its abundance of Ponderosa Pines with elevations of 1980 m to 2375 m.   The terrain drops to the east of Black Forest; however, this drop is much more pronounced to the southeast and south of the Academy.

The elevation at Limon, CO (87 km to the east-northeast) is 1635 m while at Pueblo, CO (69 km to the south-southeast) is 1440 m.
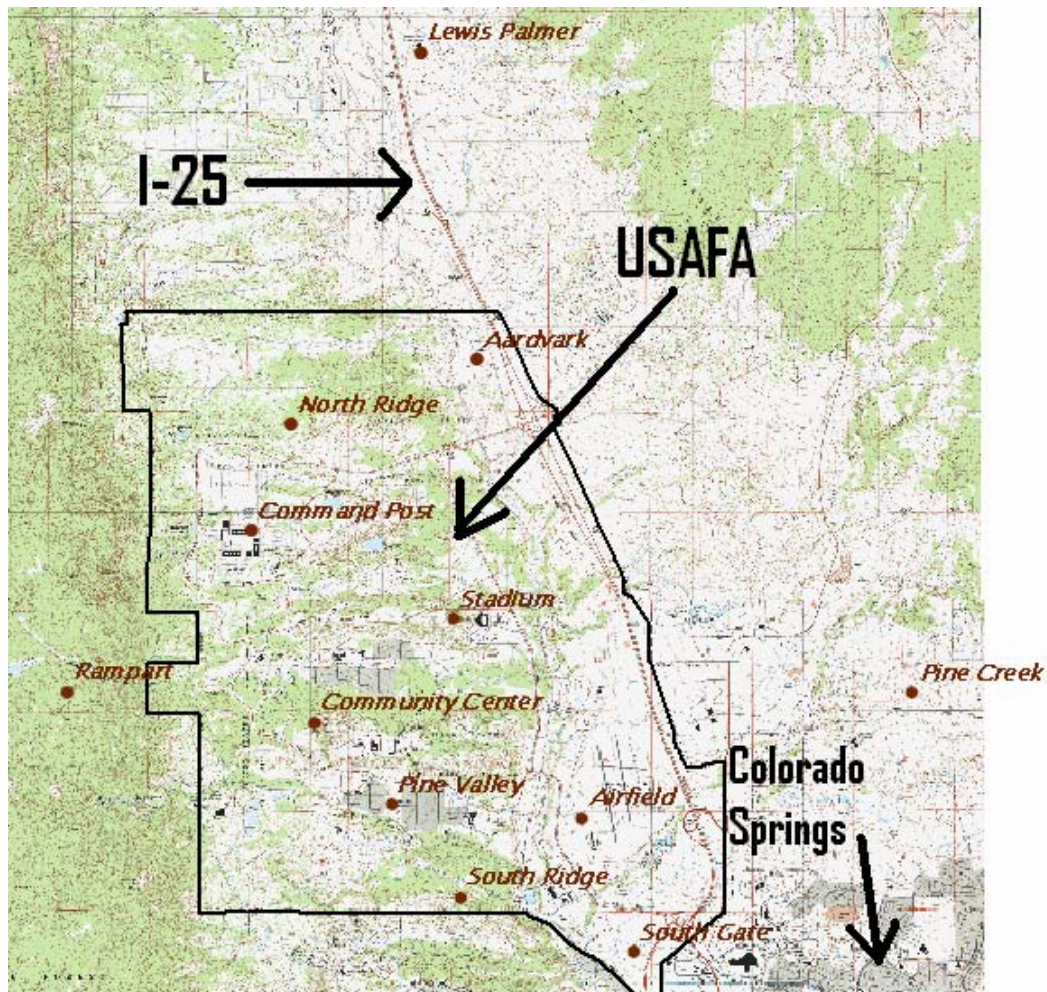
Figure 2.   Map of locations of HWAS sensors. Green shaded regions indicate areas covered by forest.

2.   High Wind Alert System (HWAS) Positioning

The 12 weather observation sensors that make up the HWAS network are strategically positioned at locations to provide an adequate sample of meteorological data and give a good representation of weather conditions around USAFA in the diverse terrain. A map of these sensors is provided in Figure 2, and the elevation and longitude/latitude positioning of each sensor is provided in Table 1. Nine of the sensors are located on the USAFA Reservation with the

Rampart sensor located at the top of the Rampart Range ridgeline due west of USAFA in Pikes Peak National Forest. The Pine Creek sensor is located on a roof at a local school east of USAFA while the Lewis Palmer sensor (also on a roof at a local school) is north of USAFA. Both of these sensors are on the edge of the Palmer Divide and the terrain decreases in elevation from these sensors towards USAFA.

Sensor Name	Latitude	Longitude	Elevation (m)
Aardvark	39° 02' 07" N	104° 50' 39" W	2042.2
Airfield	38° 56' 06" N	104° 49' 30" W	1978.2
Command Post	39° 00' 37" N	104° 53' 11" W	2179.3
Community Center	38° 58' 57" N	104° 52' 29" W	2185.4
Lewis Palmer	39° 04' 48" N	104° 51' 16" W	2132.1
North Ridge	39° 01' 33" N	104° 52' 43" W	2183.9
Pine Creek	38° 59' 12" N	104° 45' 48" W	2126.0
Pine Valley	38° 58' 13" N	104° 51' 37" W	2026.9
Rampart	38° 59' 13" N	104° 55' 14" W	2840.8
South Gate	38° 56' 56" N	104° 48' 55" W	1953.8
South Ridge	38° 57' 25" N	104° 50' 51" W	2036.1
Stadium	38° 59' 51" N	104° 50' 55" W	2084.9

Table 1.   HWAS sensors longitude/latitude and elevation.

HWAS sensors located on the USAFA Reservation are mostly located along west to east oriented ridgelines with a few exceptions. The Pine Valley sensor is on the rooftop of a school that is located in the largest west to east oriented valley on USAFA. The Airfield sensor is on the east side of Monument Creek and is located at the mouth of Pine Valley. This sensor is in an open field just west of the adjacent runways on the USAFA Airfield. The Aardvark sensor lies along the eastern most extension of the Northridge. It is adjacent to an additional runway used for training and Monument Creek. When strong winds are present from the west, because this sensor is not in a west-east oriented valley but at the base of a ridgeline, this sensor is often spared the strongest winds and the recorded wind values are much lower than at other sensors. Instead, with its proximity to Monument Creek, it is in an ideal location to

measure drainage flow from the north coming down the Palmer Divide. The only other sensor that is located on a platform that is on top of a building is the Command Post sensor which is located on top of Vandenberg Hall, a six-story tall cadet dormitory. This sensor has the greatest number of man made obstructions around it of any of the sensors with several other buildings close by in all directions. It is the furthest west and closest to the steep slopes of the Rampart Range of any of the other sensors except for Rampart which lies at the top of the Front Range.

B.   CASE STUDY-WIND EVENTS AT USAFA

Severe downslope wind events along the eastern slopes of the Colorado Rocky Mountains have been studied and well-documented for years. The primary location for these studies has been at Boulder, Colorado. The unique positioning of Boulder along the eastern slope of the Front Range of the Rocky Mountains and the close proximity of the Continental Divide west of Boulder, along with the high concentration of meteorologists and scientists working in this area have provided ample studies, papers, and documentation of these wind events. The HWAS network has recorded numerous recent downslope wind events that match or exceed many of the severe cases documented at Boulder (Brinkman, 1974). The purpose of this section is to relate and classify the type of wind events recorded during a strong downslope wind event that HWAS recorded on 6 March 2004 at USAFA. This case study will be evaluated using a triple-nested run of the MM5 (described in the next section) for the impact of the HWAS observations on analysis fields and model output fields at 12, 4, and 1.33 km. Additionally, this section will document the synoptic patterns during the wind event that HWAS recorded on 6 March 2004.

1.   Classification of Downslope Windstorms

A chinook is a foehn wind phenomenon along the eastern slopes of the Rocky Mountains. These winds are much more frequent and stronger in the winter than in the summer. The onset of a chinook is easily recognized by a

sharp increase in temperature, a drop in relative humidity, the development of strong westerly surface winds, the existence of a dry-adiabatic lapse rate, and often the appearance of wave cloud features (Oard, 1993). For a long time, severe downslope winds along the eastern slopes of the Rocky Mountains were only attributed to chinook type events. However, it has been documented that katabatic flows similar to the bora of Europe have been responsible for many of the wind events along the Colorado Front Range. Some of Boulder's windstorms have caused temperature rises of 15-20°C while others have resulted in temperature drops of up to 15°C (Brinkman, 1974). Regardless of their classification, these downslope wind events can be very intense, damaging to property, forests, vegetation, military and aviation operations, and human life. Wind intensities vary upon small-scale terrain effects, exposure, and the synoptic weather patterns and atmospheric dynamics present. Exposed locations around Boulder experience gusts at or above hurricane force several times each winter and above 50 m/s about every two years. One such severe windstorm in the Boulder area on 11 January 1972 caused an estimated $2 million in property damage (Klemp and Lilly, 1974). In 2004 alone, the HWAS at USAFA observed nine separate wind events with winds greater than 25 m/s and approached hurricane level winds with a gust of 38 m/s during one such event.

Several theories explaining the dynamic set-up of these storms have been published throughout the years and not without disagreement and controversy. Scorer and Klieforth (1959), and Aaneson (1965) proposed the generation of such winds were primarily attributed to rather short (generally <20 km wavelength) quasi-periodic lee waves that propagate downstream of a mountain range under conditions which allow trapping of wave energy to create strong windstorms. Clark and Peltier (1977) further explored this idea and suggested that large-amplitude waves and downslope winds are produced after a developing wave breaks; the energy in the upward propagating wave is trapped beneath its own level of "supercritical steepening", producing a substantial increase in the wave amplitude. Others have described the downslope windstorms on the basis of hydraulic jump theory, assuming the atmosphere can

be modeled as two or more neutrally stratified layers with sharp inversions at each layer interface. (Kuettner, 1959; Houghton and Isaacson, 1968; Arakawa, 1969). Additional work was done in this area proposing that strong winds will occur along the lee slope when a fluid undergoes a transition from subcritical flow upstream to supercritical flow over the mountain (Smith, 1977; Durran 1986; Durran and Klemp, 1987). Still a third theory emerged and suggests that strong downslope winds occur when the atmosphere has a multilayer structure which produces an optimal superposition of upward and downward-propagating waves (Klemp and Lilly, 1975).
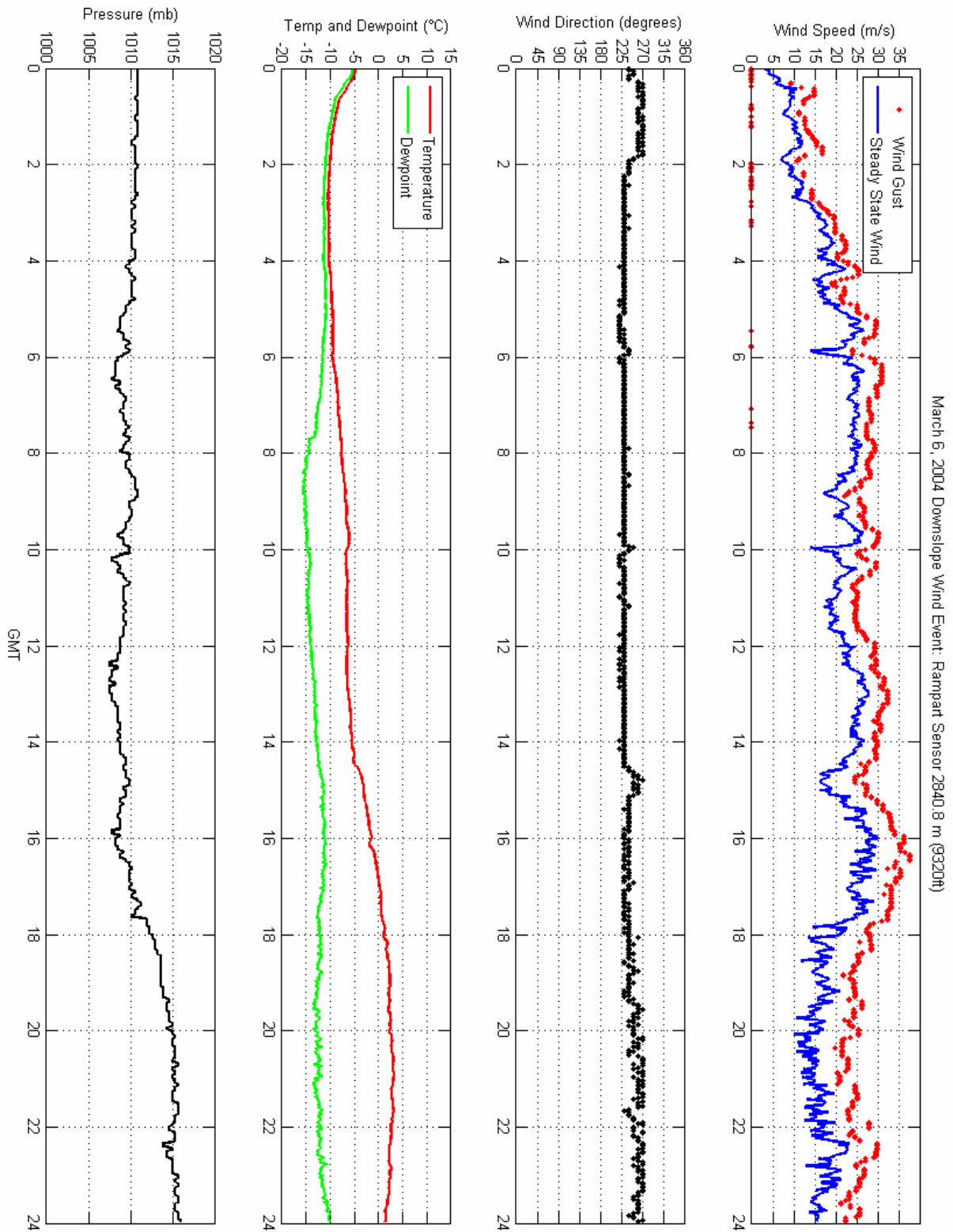
Figure 3.   Time series plot from the HWAS Rampart Sensor for 6 March 2004.

2. USAFA- 6 March 2004 Downslope Windstorm

At around 0400 UTC on 6 March 2004 a severe downslope windstorm began at USAFA that produced two separate and distinct modes of gustiness and a near hurricane strength maximum gust of 38 m/s at the Rampart sensor. This downslope wind event was a classic chinook with strong westerly downslope winds, accompanied by an immediate rise in temperature, a sharp decrease in temperature, and pressure falls with the onset of the downslope winds. The Rampart sensor (situated at the top of the first crest of the Front Range at 2840 m), began a slow and steady increase in winds from the west at about 0200 UTC. The wind increased over the night hours and peaked in the early morning hours on 6 March at about 1615 UTC (Figure 3). These strong winds lasted for about 20 hours. The warming and drying trend was not as evident at the Rampart sensor (since it is at the top of the mountain crest), as it was at sensors at lower elevations that experienced compressional warming of the air as it was forced down the mountain slopes.

The Community Center sensor (which was representative of all the other sensors that were in the 2000 to 2200 m elevation range) had a sharp change in wind direction from the south to the west at 0400 UTC and quickly began to gust routinely above 25 m/s (Figure 4). This sharp increase in winds brought a 5°C temperature rise and a 9°C drop in dewpoint over the next hour. A strong temperature inversion existed between the sensors in higher terrain and the sensors at lower elevations. This caused the strong winds to stay above the inversion and slowly mix down to the lower terrain over the next several hours. Above the inversion, situated at about 2200 m at 0500 UTC, winds continued to gust, temperatures rose, pressures fell, and dewpoints dropped. Under the inversion, winds were generally weak and out of the southeast, pressures were falling very slowly, and conditions were near saturation as evident at the Airfield and South Ridge sensors (not shown). The high winds above the inversion slowly mixed down to even the lowest sensors by 0800 UTC, and these stations exhibited the classic chinook weather pattern with high winds (although not as high as sensors at higher elevations) for the next 12-24 hours.
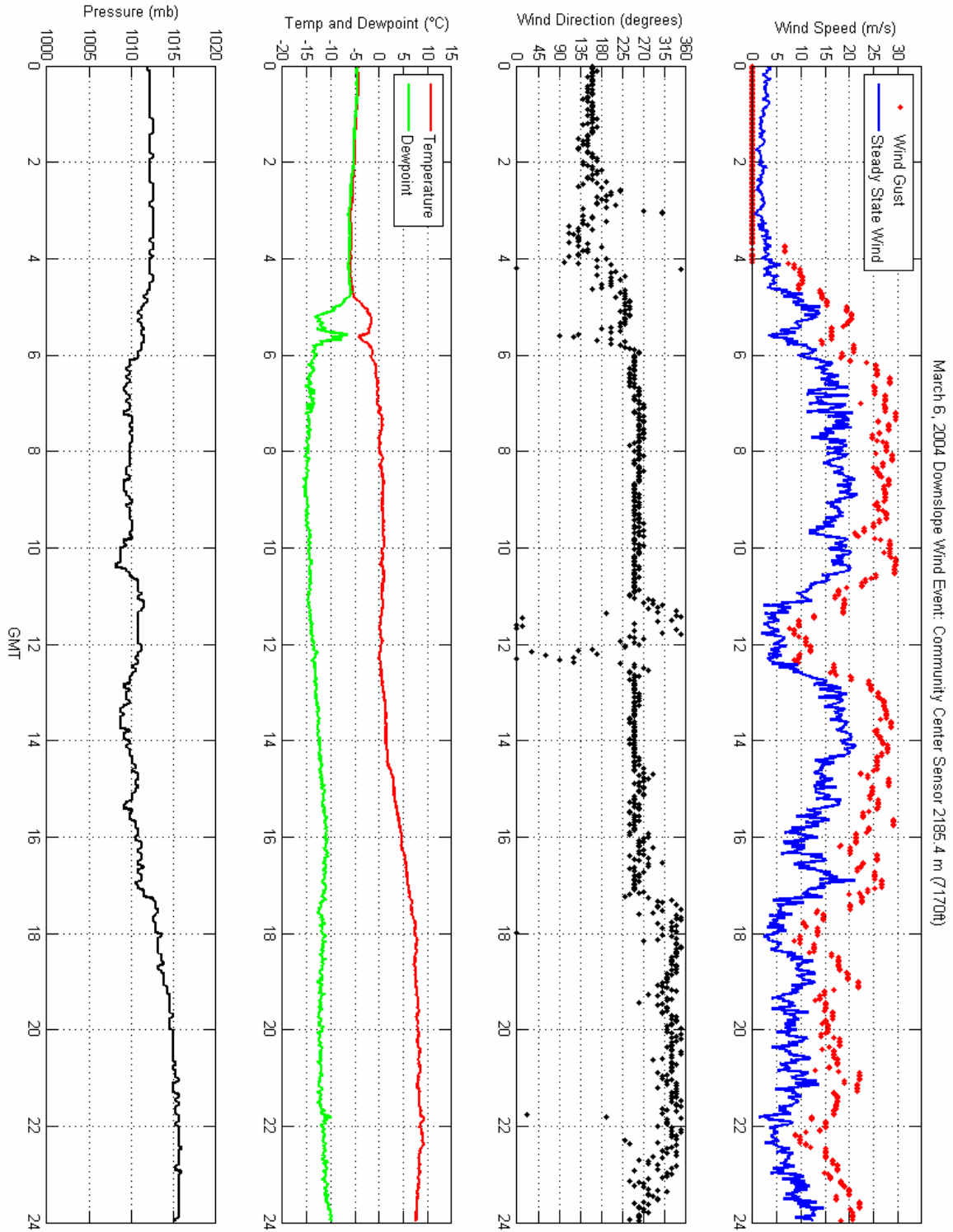
Figure 4.   Time series plot from the HWAS Community Center Sensor for 6 March 2004.
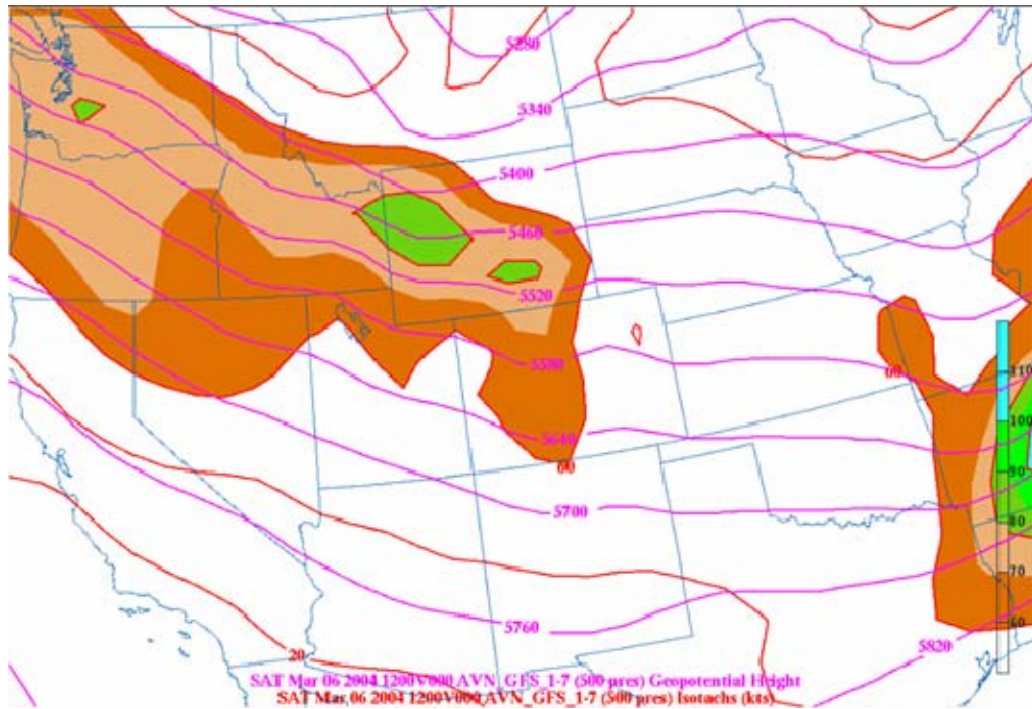
Figure 5.   500 mb heights and winds (kt) from the GFS 6 Mar 2004 1200 UTC analysis.
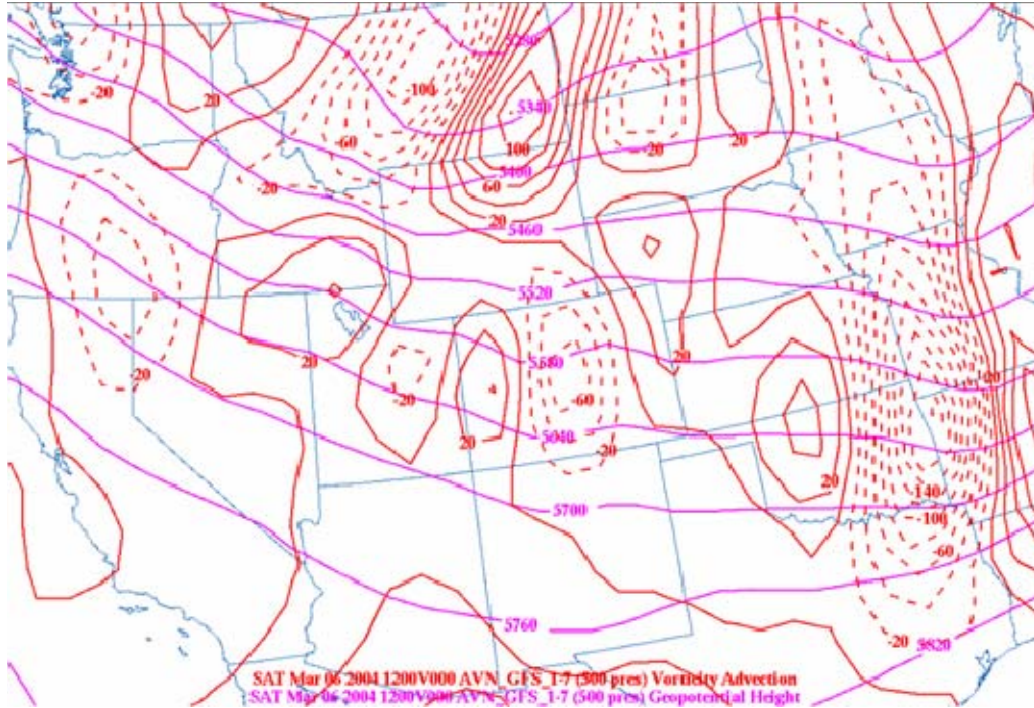
Figure 6.   500 mb heights and vorticity advection from the GFS 6 Mar 2004 1200 UTC analysis.

3.   Synoptic Overview of the 6 March 2004 USAFA Windstorm

During this event a strong upper level ridge existed over the eastern Pacific with a weak upper level trough over the Mississippi Valley. This created strong 500 mb flow from the northwest to the southeast across the western half of the contiguous United States. Embedded in this northwest flow were several shortwave troughs, but no major baroclinic waves. At 1200 UTC the 500mb GFS analysis (Figure 5) showed a shortwave trough over central Colorado with a wind max of 80 kt to the north over Wyoming. An area of coupled positive and negative vorticity advection was analyzed by the GFS associated with this shortwave trough with the negative vorticity advection over the eastern slopes of the Rockies during the peak of the 6 Mar USAFA windstorm (Figure 6).
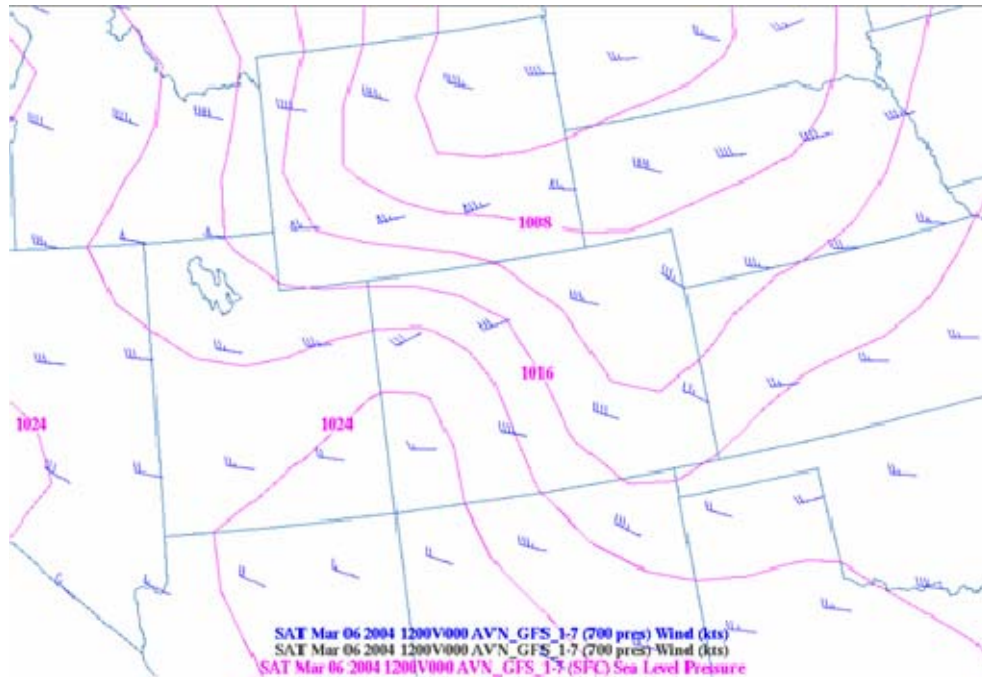
Figure 7.   Mean Sea Level Pressure and 700 mb winds (kt) from the GFS
6 Mar 2004 1200 UTC analysis.

A strong surface pressure gradient (between 850-700 mb over elevated terrain in Colorado) and strong westerly winds of around 40 kt were analyzed by the GFS for this same time period over central Colorado (Figure 7). This indicates that the GFS (a global model) had a good handle on the timing of this wind event over Colorado and even a reasonable depiction of the magnitude of the steady state winds or synoptic flow for this event, but it is speculated that due to the coarse spectral resolution and smoothed terrain representation, the highest winds over the downsloping terrain in the area around USAFA were not very well depicted.

At 700 mb a very interesting wave pattern emerges (Figure 8). The alternating upward and downward pattern depicted in the 700 mb omega fields from the northwest to the southeast in a line from Washington to the Texas Panhandle indicate that a large-scale mountain wave feature was present across almost the entire western United States. The GFS indicates this was a standing

30

wave and not a propagating feature since it persisted with very little movement from about 0600 UTC 6 Mar until about 0000 UTC 7 Mar. A cross section of this feature is depicted in Figure 9.
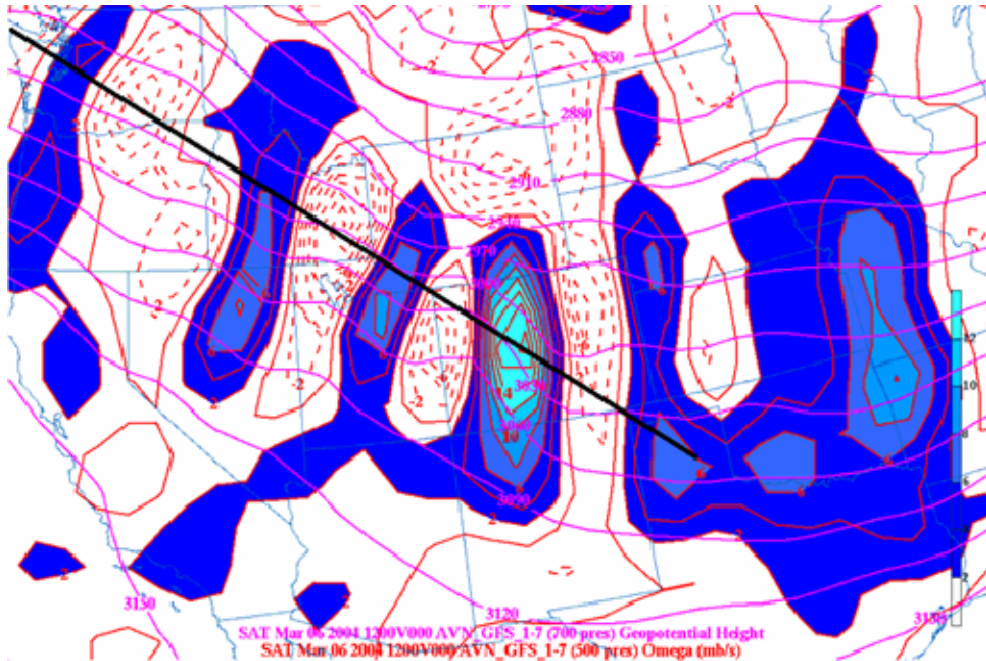
Figure 8.   700 mb heights and omega (mb/s) from the GFS 6 Mar 2004
1200 UTC analysis. Black line indicates path of cross section
depicted in Figure 9.
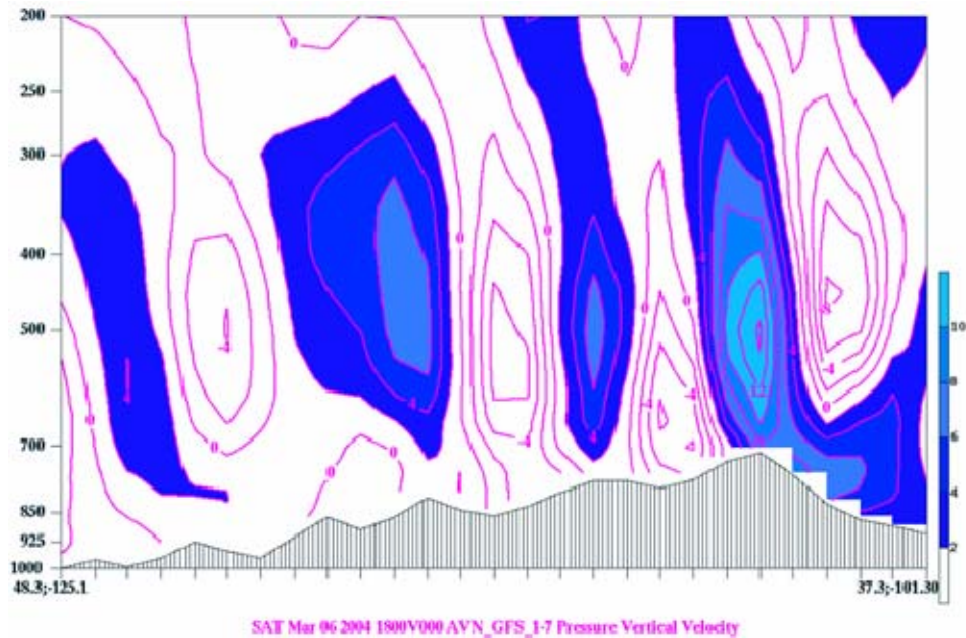
Figure 9. Cross section along path shown in Figure 9 showing the GFS model's representation of topography and omega (mb/s) for the 6 Mar 2004 1200 UTC analysis.

C. DATA

1. HWAS Data

HWAS is a network of 12 automated, solar-powered sensors that measure surface winds, temperature, relative humidity, and pressure every 2 minutes located on and around USAFA in Colorado Springs, Colorado. A continuous set of HWAS data extends back to 1 Jan 2004. The exact positioning and elevation, longitude, and latitude information is show in Table 1 and Figure 3. Pictures of examples of the types of sensors and mounting positions of different HWAS sensors are shown in Figure 10. Real-time HWAS observations are available at http://www.usafa.af.mil/df/dfeg/meteorology/hwasinfo.cfm?catname=dfpm.

2. Meteorological Assimilation Data Ingest System (MADIS) Data

MADIS is a dataset maintained and made available by the National Oceanic and Atmospheric Administration's (NOAA) Earth System Research Laboratory (ESRL) Global Systems Division (GSD) (formerly the Forecast Systems Laboratory (FSL) for the purpose of improving weather forecasting, by

providing support for data assimilation, numerical weather prediction, and other hydrometeorological applications. Real-time and archived MADIS data is available at http://madis.noaa.gov. MADIS surface observations are a compilation of reports from many observing networks run by different "providers". These include all stations that report standard METARs (ASOS, AWOS, non-automated stations), as well as modernized (i.e., automated) National Weather Service Cooperative Observer reports. Altogether about 300 MADIS surface observations from the state of Colorado are used in this study. They include weather observations from sensors run by the Colorado Avalanche Information Center (CAIC), Colorado Department of Transportation (CDOT), Remote Automated Weather Stations (RAWS), Citizen Weather Observers Program (APRSWXNET), as well as many other similar networks across the state of Colorado to include all METAR reports. The USAFA HWAS network is now a part of the MADIS data set; however, it was not included at the time of the case studies that are apart of this research from 2004.

Figure 10.   Picture of the Pine Creek HWAS sensor (top) and the Rampart HWAS sensor (bottom).

3. Radiosonde Data

Radoisonde data (often referred to as RAOB's) archived at the Naval Postgraduate School (NPS) Department of Meteorology were used for this study in the data assimilation process described in the next section.

4. ETA Model Data

ETA model data from the ETA 212 with 12 km resolution was archived at the NPS Department of Meteorology for the western CONUS and was used in this study. The archived ETA model data from 2004 has an initial analysis time and model forecasts every three hours out to 84 hours. It also has model runs every six hours with model forecast start times of 00, 06, 12, and 18 UTC.

D. METHODS

A nested-grid structure was created for analysis and input to the MM5 model with the coarsest grid horizontal resolution set at 12 km, an intermediate grid set at 4 km, and the finest grid set at 1.33 km. Terrain data was input at 10 minutes for the 12 km grid, and 30 second terrain data was input for the 4 and 1.33 km grids. The grid dimensions for the 12 km grid were 151 x 133, with the 4 km grid 121 x 109, and the 1.33 km grid 103 x 97. All three grids were centered over USAFA at a latitude/longitude of 39.0 N, -104.9 W (See Figure 11).

Analyses using the ETA 212 12 km as a first guess were created using Three Dimensional Multiquadric Interpolation (3DMQ) and assimilating all available RAOB's, MADIS surface observations, and HWAS observations at one hour intervals starting at 00 UTC on 6 March 2004 through 00 UTC on 7 March 2004 for the 12, 4, and 1.33km grids. These same analyses were then performed again exactly the same, except the HWAS observations were left out in the analysis process. Verification statistics and difference fields were generated for comparison between the analysis fields with the HWAS observations and without the HWAS observations. All observations within 100 m/s of the ETA first guess field were allowed to remain in the analyses during the

quality control portion of the data assimilation process. The purpose of this was to maximize observation input for the wind fields and not have any wind observations kicked out of the analyses. More standard error thresholds were used for observations and their other weather variables during the quality control portion of the data assimilation process.
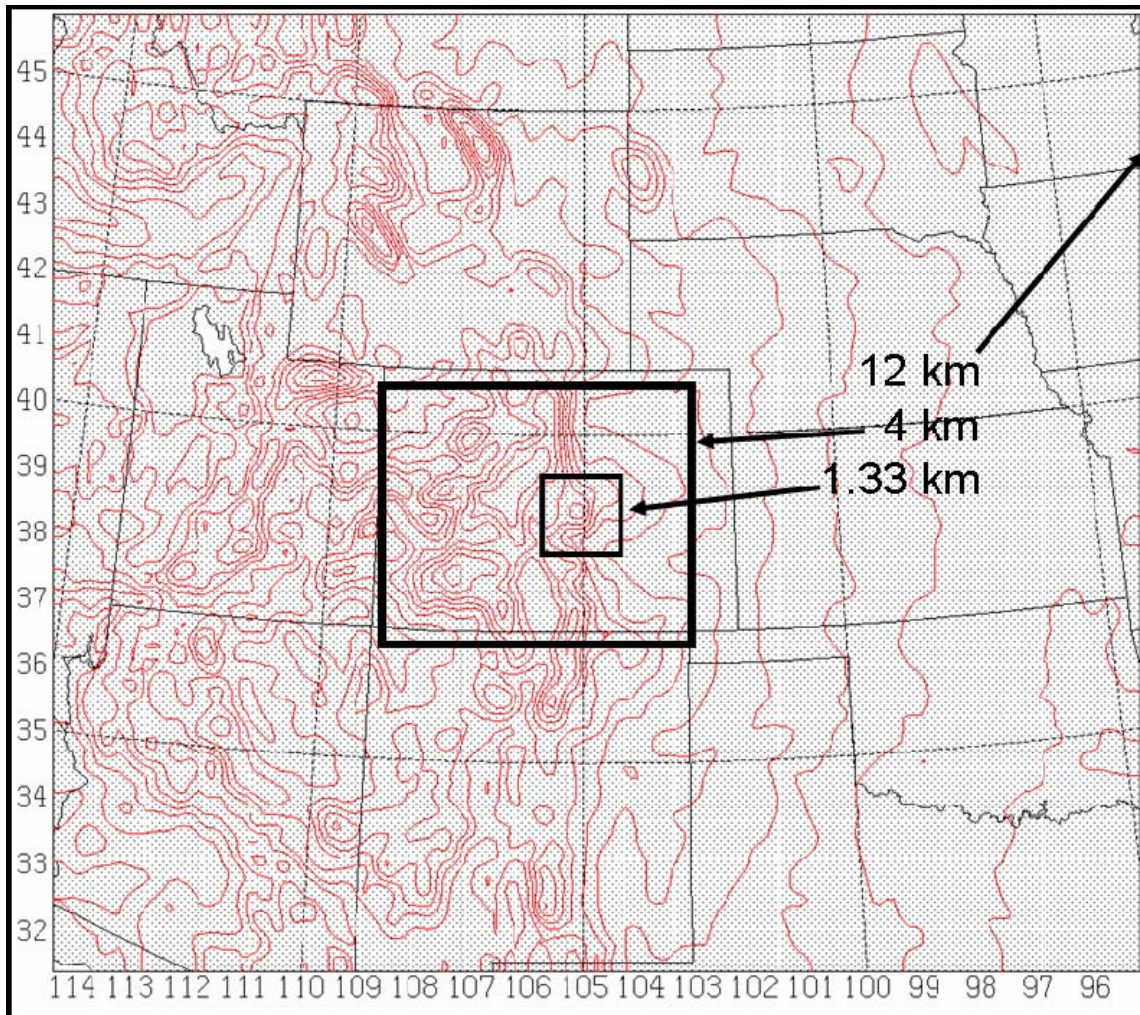
Figure 11.   Map of the 12, 4, and 1.33 km nested domains with terrain elevation contoured at 250 m.

The analyses as just described were then used as the initial conditions for the triple-nested MM5 model runs. Model runs were created for 18 UTC on 5 March and 00 UTC and 06 UTC on 6 March 2004 with forecasts out 30, 24, and 18 hours respectively with all model runs ending at 00 UTC on 7 March 2004.

The analyses with HWAS observations included were used as the initial conditions for the first three model runs, and then the same model runs were produced a second time with the analyses without the HWAS observations included used as initial conditions. Verification statistics and difference fields were generated for comparison between the models fields with the HWAS observations included in the analyses used as the initial conditions and model fields without HWAS observations included in the analyses.

1.   3DMQ

All analyses performed in this study were done with 3DMQ, a three dimensional interpolation scheme developed initially in two dimensions (Nuss and Titley 1994) and most recently in three dimensions (Nuss 2007). 3DMQ was used to combine the scattered RAOB, MADIS, and HWAS observations at differing elevations into a full three dimensional analysis (12, 4, and 1.33 km) fitted to a 3D grid using the three dimensional ETA model 12 km as a first guess field. The benefit of using the 3DMQ interpolation scheme is that by fitting the observations to a regular grid, verification statistics and difference fields between the analyses that include HWAS observations and those that do not can be performed. In addition, by creating the three dimensional fields in this manner, analyses could be interrogated using VISUAL for meteorological and computational fields, and also easily adapted to be used as the first guess fields for the initialization in MM5 model runs.

Nuss and Titley (1994) showed that multiquadric interpolation, which uses hyperboloid radial basis functions, is better than several other interpolation schemes at fitting scattered data to uniform grids while retaining small-scale features resolved by the observations. Additionally, they demonstrated the enhanced accuracy of multiquadric interpolation over Barnes and Cressman interpolation schemes with meteorological observations spread over various boundaries similar to the boundaries observed between the mountainous regions and plains of Colorado.

The interpolation equation using radial basis functions is:

$$H(X) = \sum_{i=1}^{N} \alpha_i Q(X - X_i) \quad (3.1)$$

where $H(X)$ is a spatially varying field such as wind (U, V) or temperature and $Q(X - X_i)$ is a radial basis function where $Q(X - X_i)$ represents the vector between an observation point X_i and any other point in the domain. The coefficient α_i is a weighting function that must be specified. The multiquadric method uses hyperboloid basis functions in the form:

$$Q(X - X_i) = -\left(\frac{(X - X_i)^2}{c^2} + 1.0 \right)^{\frac{1}{2}} \quad (3.2)$$

where c is an arbitrary and typically small constant called the multiquadric parameter. For 3DMQ X represents the position vector in three dimensions.

When applying this technique to meteorological observations, a problem can arise when errors due to a partial sampling of small-scale features can result in an unrealistic analysis. Observation error can be addressed using a smoothing parameter λ that filters unresolved scales from the analysis. Different observation sources can cause observation error to be varied with the result that the analysis will fit more closely to some observations than others. In this study, less error was assigned to the actual observations than to the ETA model first guess fields.

A script called run3dmq organizes the input fields and creates the output fields for 3DMQ. 3DMQ requires an analysis time and first guess times that the ETA first guess fields are pulled from. If a 3DMQ analysis time does not fall on one of the ETA initial analysis times (00, 06, 12, 18 UTC), then the first guess field from the ETA uses a forecast field (available every three hours) for the initial guess for 03, 09, 15, and 21 UTC. For example, an analysis for 00 UTC on 6 March uses the 00 hour initial field from the 00 UTC run of the ETA as the first guess field. The analysis for 03 UTC on 6 March uses the 03 hour forecasts

from the 00 UTC run of the ETA as the first guess field. If an analysis time fall at an hour not divisible by three, then a first guess field is created by linearly interpolating a 00 hour initial analysis of the ETA with a 03 hour forecast of the ETA to provide the first guess field. For example, an analysis for 02 UTC on 6 March linearly interpolates between the 00 hour ETA initial analysis for the 00 UTC run and the 03 hour forecast of the 00Z ETA run to create a 02 UTC first guess field. This process is the same for each of the grid domains created with analyses for the 12, 4 and 1.33 km done every hour during the case study for verification. Each run of 3DMQ produces output files for sea level pressure, surface pressure, geopotential height, moisture, U wind component, and V wind component. Quality control of observations are performed before they are integrated into each analysis by using a gross error check (difference between observed variable and initial first guess by the ETA model) that can be modified to allow more or less of the observations into each analysis. Additionally, if a station's observations were deemed unreliable on a semi-permanent basis, that particular observation was put on a "blacklist" and not included in the 3DMQ process.

One property that makes 3DMQ unique is that it smoothly analyzes the scales represented by the observations in one region where a lack of observations is present along a boundary or section of the domain while not producing undesired results elsewhere (Nuss and Titley 1994). This is particularly important in many of the mountainous regions of the domain where observations are often sparse yet dense around populated regions such as the front range of Colorado. 3DMQ retains the synoptic scale features at the boundaries of the domain without sacrificing resolution of mesoscale features at the center of the domain.

2. VISUAL

The VISUAL program is a FORTRAN based program developed by Professor Wendell Nuss that displays a wide variety of meteorological data and performs numerous computations on these datasets. VISUAL is based on NCAR

graphics and XGKS graphical software for plotting. The analysis grids generated by 3DMQ were displayed and investigated using VISUAL.

3.   MM5

The Mesoscale Model Version 5 Version 3 (MM5V3) is used for all model runs under investigation by this study.   The MM5 has been developed and maintained by researchers at Penn State University and at NCAR. The MM5 is a limited-area, nonhydrostatic, terrain-following sigma-coordinate model designed to simulate or predict mesoscale atmospheric circulation (UCAR MM5 Community Model, 2006).   For this study a triply-nested MM5 model was designed with the coarsest grid horizontal resolution set at 12 km, an intermediate grid set at 4 km, and the finest grid set at 1.33 km. Terrain data was input at 10 minutes for the 12 km grid, and 30 second terrain data was input for the 4 and 1.33 km grids. The lateral and initial boundary conditions for all grids come from the 3DMQ data assimilation process as described in previous sections. Each nest of the model is run at 30 sigma levels with the time step set at 36 seconds for the 12 km domain, 12 seconds for the 4 km domain, and 4 seconds for the 1.33 km domain. The near ground sigma surfaces closely follow the terrain, while at upper levels the sigma surfaces tend to approximate isobaric surfaces. The majority of the sigma levels are used to describe the atmosphere between the surface and 700mb. An advantage of using sigma surfaces over pressure or height surfaces is the fact that sigma surfaces do not intersect terrain as other surfaces do (UCAR MM5 Community Model, 2006).

IV. RESULTS

This chapter summarizes the results of the analyses that were created using the ETA 212 12 km as a first guess field and using 3DMQ to assimilate all available RAOB's, MADIS surface observations, and HWAS observations at one hour intervals starting at 00 UTC on 6 March 2004 through 00 UTC on 7 March 2004 for the 12, 4, and 1.33 km grids. Additionally, this chapter presents the results of the MM5 model runs that were created for 18 UTC on 5 March and 00 UTC and 06 UTC on 6 March 2004 with forecasts out 30, 24, and 18 hours respectively with all model runs ending at 00 UTC on 7 March 2004. Six model runs were done in total, with three using analyses that included HWAS observations for initial conditions, and three that did not use HWAS observations in the analyses used for initial conditions.

Through the use of difference fields and Root Mean Square Error (RMSE) calculations the impact of the HWAS observations on the various grid sizes using 3DMQ and the forecast fields of the MM5 were investigated. Using a tool within the VISUAL program, surface steady state wind speed values in m/s at each HWAS observation location were extracted for both the analysis fields and the model forecast fields. These values were used along with the actual recorded data from the HWAS observations to produce RMSE statistics for each hour investigated at each of the HWAS observation locations. RMSE or other verification statistics were not produced for any other locations within the grid domains. For the purposes of this study, only steady state wind speed, independent of wind direction and wind gusts, was taken into account for verification statistics.

A.   3DMQ ANALYSES

Determining the differences between the analyses done on each of the respective grid sizes and the analyses done with and without HWAS observation data is the first step in understanding how well 3DMQ performed at fitting the available observations to the first guess fields. Additionally, by determining the

RMSE at each of the HWAS locations during the high wind event in the case study, an understanding of the accuracy of the analyses with and without the HWAS observations included can be ascertained.

1. HWAS Observation Included

TIME(UTC)	1.33 km	4 km	12 km	AVERAGE
040306/0000	0.6089	0.8750	1.1361	0.8733
040306/0100	1.6515	2.0741	2.2284	1.9847
040306/0200	1.7367	2.1074	2.2669	2.0370
040306/0300	3.1626	3.9792	4.2461	3.7960
040306/0400	3.5234	4.3171	4.3623	4.0676
040306/0500	4.6317	5.4126	5.6786	5.2410
040306/0600	5.0247	5.8284	5.8601	5.5711
040306/0700	5.9284	6.6704	6.7503	6.4497
040306/0800	5.6801	6.7448	6.9890	6.4713
040306/0900	4.9701	6.0210	6.3848	5.7920
040306/1000	3.7000	4.3176	4.2039	4.0738
040306/1100	4.5306	5.2728	5.3269	5.0434
040306/1200	4.1152	5.5190	6.0029	5.2124
040306/1300	6.6445	7.7778	8.4944	7.6389
040306/1400	6.6050	7.7457	8.4114	7.5874
040306/1500	4.5976	5.9015	7.4113	5.9702
040306/1600	5.6911	6.6524	6.7799	6.3745
040306/1700	4.2861	4.9832	4.9353	4.7349
040306/1800	3.9425	4.7770	4.8831	4.5342
040306/1900	3.6381	3.9749	3.7407	3.7846
040306/2000	2.8456	3.2027	3.3013	3.1165
040306/2100	2.6796	2.9176	3.0776	2.8916
040306/2200	3.0701	3.8099	4.0067	3.6289
040306/2300	3.0384	3.3032	3.1193	3.1536
040307/0000	3.5648	4.6508	6.0607	4.7587
AVERAGE	3.9947	4.7534	5.0263	

Table 2.   RMSE by hour and grid resolution for wind speeds at HWAS observations locations for 3DMQ analyses performed with HWAS observations included from 00 UTC 6 March through 00 UTC 7 March 2004. Wind speeds used to perform calculations are in m/s.

Figure 12.   Graph showing RMSE by hour for 1.33, 4, and 12 km analyses including HWAS observations from 00 UTC 6 March through 00 UTC 7 March 2004. Red line depicts the average wind speed by hour for all HWAS sensors.

Table 2 displays RMSE statistics generated at all HWAS locations by hour and grid size from 00 UTC on 6 March through 00 UTC on 7 March 2004 during the high wind event at USAFA. Data from the HWAS observations was included in the analyses done for the RMSE statistics shown in Table 2. The RMSE average of all hours combined for the 1.33 km grid of 3.9947 was significantly better than either the 4 km or 12 km domains. When looking at each hour individually, the 1.33 km analysis performed better than the 4 and 12 km analyses at every analyzed hour. While the 4 km analyses performed better than the 12 km analyses overall, the separation between the RMSE for the 4 and 12 km was not as great as the separation between the 1.33 and 4 km. In fact, there

were many hours with only minute differences between the 4 and 12 km RMSE and four hours where the 12 km performed better than the 4 km analyses (10, 17, 19, 23 UTC).

Figure 12 displays a plot with time of RMSE for the various grid sizes of the data from Table 2 and clearly demonstrates the 1.33 km grid analyses superiority over the other two resolutions tested. Additionally, Figure 13 shows the correlation on all grid resolutions between the average wind speed for all the HWAS sensors and the magnitude of the RMSE error. In general, as the wind speed increases, the RMSE at all resolutions increase, and when the wind speed decreases the RMSE at all resolutions decrease. The relationship between the average wind speed and the various grids RMSE indicate the performance of the ETA 212 12km model that was used as a first guess field before adding soundings and surface observations during this strong downslope windstorm. Although there was some temporal variability among the HWAS sensors, there were two main wind maximums during the windstorm around 09 UTC and 15 UTC with a lull in between around 12 UTC.

The correlation between the RMSE values and the average wind speed indicates the inability of the HWAS observations to completely correct for a bad forecast given by the ETA model used as the first guess field before data assimilation. The ETA model clearly underforecasted the intensity of the first peak of winds around 09 UTC and slowly increased the winds throughout the day causing it to cause the better RMSE values late in the day. A close examination of the ETA forecast fields for this event showed the ETA model slowly increased winds throughout the day and kept them at moderate levels at all locations without the lull around 12 UTC. Adjusting first guess fields with the HWAS and other observations was clearly not enough to create an accurate analysis due to the poor first guess field provided by the ETA. The high RMSE values during some of the hourly analyses indicate that 3DMQ does not over-weight observations in its data assimilation process, but rather uses them to nudge first guess fields towards better although not perfect analyses. Weighting

44

observations too highly could potentially lead to a more accurate local analysis, but cause detrimental effects in the transition zones between areas with a high density of observations and areas with sparse observations. Abrupt changes in analysis fields could actually lead to an overall degradation of verification when the entire grid domain is taken into account and also cause unintended errors in model runs when these analyses are used as initial conditions.

SENSOR	1.33 km	4 km	12 km	AVERAGE
Aardvark	1.3647	1.7042	2.0961	1.7216
Airfield	2.2371	2.0891	2.7441	2.3568
Command Post	4.1983	5.5793	5.8996	5.2257
Community Center	5.8296	6.2364	6.4550	6.1737
Lewis Palmer	1.4813	1.7337	1.8763	1.6971
North Ridge	3.6431	4.3334	4.9591	4.3119
Pine Creek	3.4855	4.0823	4.1525	3.9068
Pine Valley	2.5127	2.3916	3.0011	2.6351
Rampart	10.5596	13.0877	13.3849	12.3441
South Gate	1.4839	1.7674	2.3883	1.8799
South Ridge	2.9220	2.5970	3.2678	2.9289
Stadium	1.7523	2.0539	2.8055	2.2039
AVERAGE	3.4558	3.9713	4.4192	

Table 3.   RMSE by sensor and grid resolution for wind speeds at HWAS observations locations for 3DMQ analyses performed hourly with HWAS observations included from 00 UTC 6 March through 00 UTC 7 March 2004. Wind speeds used to perform calculations are in m/s.
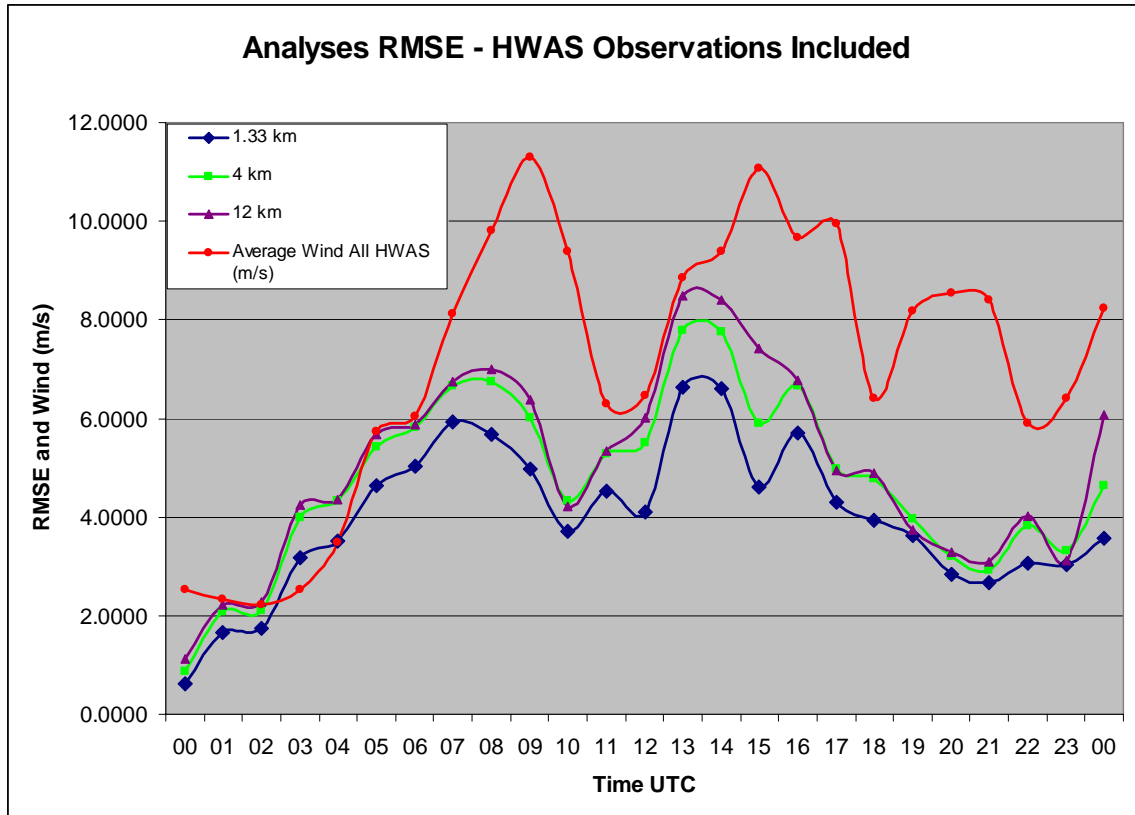
Table 3 depicts RMSE statistics generated from all HWAS locations by sensor and grid size from 00 UTC on 6 March through 00 UTC on 7 March 2004 during the high wind event at USAFA. The wind speed data from the HWAS observations were included in the analyses done for the RMSE statistics shown in Table 3. This second perspective of the RMSE values confirms many of the same results as when they are viewed by hour. Again, the 1.33 km analysis grids performed the best overall followed by the 4 km and the 12 km analysis grids with a greater separation between the 4 and 12 km grids when viewed by sensor, rather than by hour. At every sensor the 1.33 km RMSE was smaller than at 4 km and this is also true for the 4 km when compared to the 12 km.
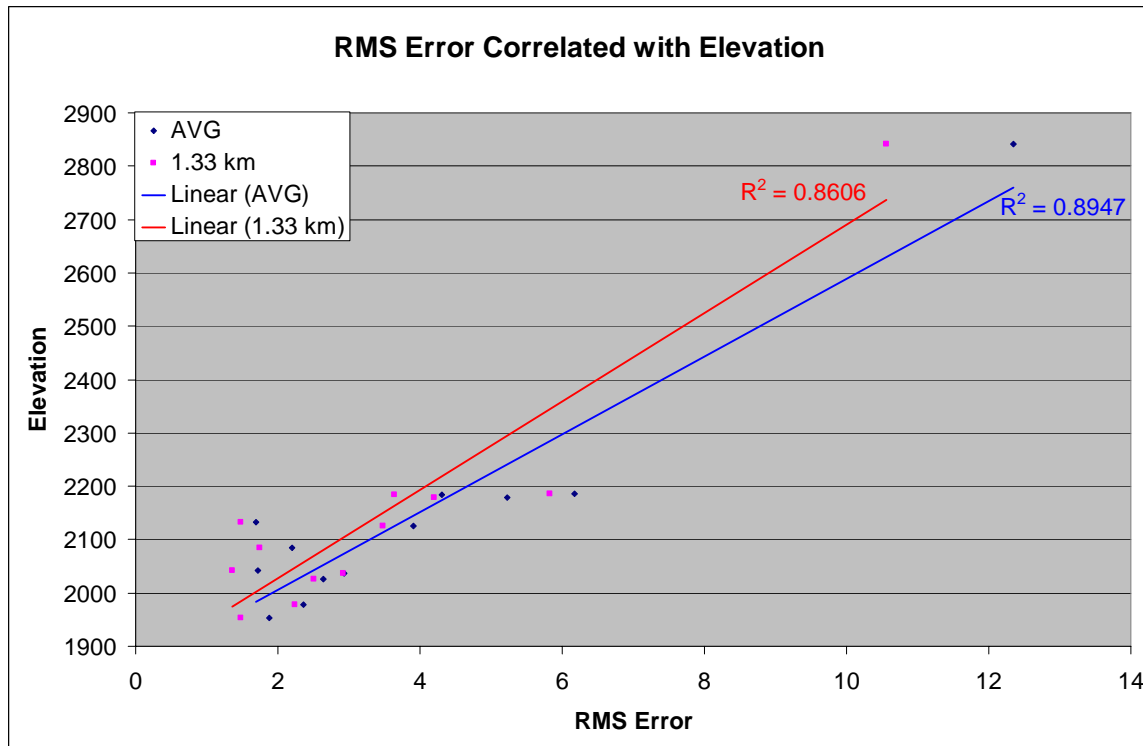
Figure 13. RMSE correlated with elevation for the 3DMQ analyses with HWAS observations included.

When looking at the average RMSE by sensor including all three grid sizes, Lewis Palmer performed best with an overall RMSE of 1.6971 for all 24 hours followed closely by Aardvark. The Rampart sensor had highest RMSE values at all grid sizes with an overall average of 12.3441. A hourly graph of actual steady state wind observations for the Rampart sensor versus 1.33 and 12 km analyzed values with HWAS observations included is shown in Figure 14 and clearly shows the 1.33 km analyzed values are better than the 12 km analyzed values for most hours, but neither does an adequate job overall depicting the actual magnitude of the wind. Other sensors higher in elevation also had larger RMSE, while many of the lower elevation sensors had much smaller RMSE. The correlation between elevation and RMSE is shown in Figure 13 and clearly demonstrates that sensors higher in elevation verified poorly with respect to RMSE when compared to sensors at lower elevations. The biggest outlier to this correlation is the Lewis Palmer sensor, which lies at 2132.1 m yet had the best RMSE overall. The topography around Lewis Palmer is unique as it lies near the

top of the Palmer Divide and is the northern most of the HWAS sensors. It's elevation is comparable to the Command Post and Community Center sensors (2179.3 and 2185.4 m), yet it experienced much lower wind speeds with the highest steady state winds around 10 m/s with gusts only to 15 m/s. In contrast, both the Command Post and Community Center sensors had steady state winds around 16-18 m/s with gust as high as 27 m/s.

Rampart - HWAS Included
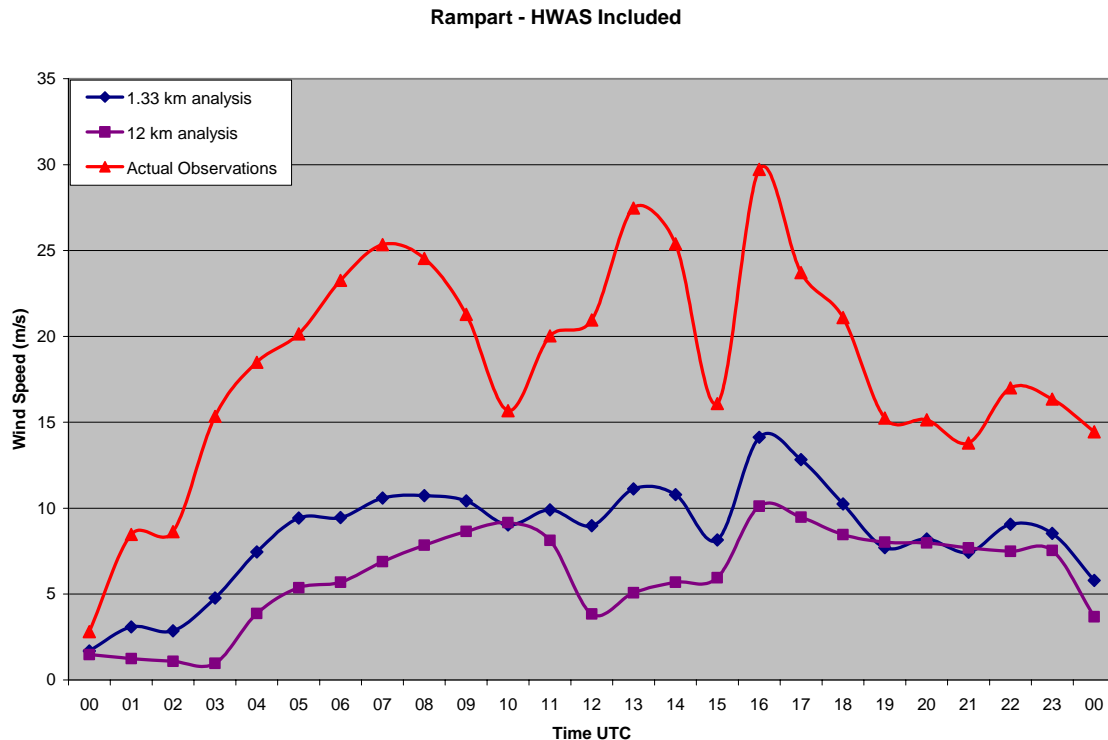
Figure 14.   Graph of hourly steady state wind observations for the Rampart sensor versus 1.33 and 12 km analyzed values with HWAS observations included for 00 UTC 6 March through 00 UTC 7 Mar 2004.

The lower observed winds and RMSE values at Lewis Palmer indicate the strongest winds did not extend as far north as the Palmer Divide. Also, the winds forecasted by the ETA model, used as a first guess field, were more on the order of the winds observed at Lewis Palmer across the entire region thus why Lewis Palmer verified well in the analyses while other locations with similar elevations experienced much higher winds and verified poorly. The high RMSE values at

most other sensors at higher elevations indicate that the highest winds were mostly experienced at the higher elevations as is common in downslope windstorms and verified by the data recorded by the HWAS sensors. The combination of the ETA model underforecasting the peak winds of the mountain wave that initiated the downslope windstorm, especially in the higher elevations, and the desire to not over-weight observations in the initial analyses while adjusting the first guess fields, caused high RMSE values to be recorded at numerous times and locations despite including the HWAS observations in the data assimilation process.

TIME(UTC)	1.33 km	4 km	12 km	AVERAGE
040306/0000	0.6565	0.6831	0.9480	0.7625
040306/0100	2.0874	2.1406	2.1469	2.1250
040306/0200	2.2170	2.2220	2.2941	2.2443
040306/0300	4.0656	4.2171	4.3151	4.1992
040306/0400	4.5965	4.6171	4.3559	4.5232
040306/0500	6.2548	6.3070	5.8325	6.1314
040306/0600	6.6910	6.4998	5.9446	6.3785
040306/0700	8.3409	7.8353	6.9564	7.7109
040306/0800	9.1945	8.5013	7.5094	8.4018
040306/0900	9.2911	8.2596	7.0579	8.2029
040306/1000	5.4722	5.0075	4.3724	4.9507
040306/1100	5.9022	5.5826	5.3632	5.6160
040306/1200	5.2839	5.6903	5.9126	5.6290
040306/1300	8.4534	9.0501	9.0356	8.8464
040306/1400	9.1869	9.2643	8.8321	9.0945
040306/1500	7.4557	8.2191	8.5834	8.0861
040306/1600	7.7902	7.4983	6.9214	7.4033
040306/1700	6.0498	5.8430	5.0474	5.6467
040306/1800	5.1860	5.1344	5.0884	5.1363
040306/1900	4.6970	4.2798	3.7229	4.2332
040306/2000	3.8757	3.4214	3.3544	3.5505
040306/2100	3.6518	3.1581	3.1932	3.3344
040306/2200	4.2037	4.4410	4.1423	4.2624
040306/2300	4.2395	3.7005	3.1631	3.7011
040307/0000	5.4902	6.0986	7.0731	6.2207
AVERAGE	5.6133	5.5069	5.2467	

Table 4.   RMSE by hour and grid resolution for wind speeds at HWAS observations locations for 3DMQ analyses performed without HWAS observations included from 00 UTC 6 March through 00 UTC 7 March 2004. Wind speeds used to perform calculations are in m/s.

2.   HWAS Observations Not Included

Table 4 displays RMSE statistics generated at all HWAS locations by hour and grid size from 00 UTC on 6 March through 00 UTC on 7 March 2004 during the high wind event at USAFA. Data from the HWAS observations was not included in the analyses done for the RMSE statistics shown in Table 4. In complete contrast to the RMSE statistics generated for the same locations and same time periods with HWAS observations, the overall average RMSE increased as grid size decreased. The 12 km grid domain performed the best with an overall RMSE average of 5.2467 over all hours, only slightly worse than the 5.0263 RMSE when the HWAS observations were included in the analyses. Surprisingly, the 1.33 km grid verified the worst with an overall RMSE average of 5.6133 over all hours.

The 1.33 km showed the largest change between the analyses with the HWAS observations included and those without with an overall difference of 1.6186 RMSE. The hour with the largest difference between the RMSE on the 1.33 km for the analysis done with the HWAS observations included and without is 09 UTC on 6 March 2004. The difference or contribution to the analysis by adding the HWAS observations to the analysis for 09 UTC is depicted in Figure 16. The strong winds present over USAFA at this time correspond to the first peak of wind gusts during this storm and again indicate the ETA model's, which was used as a first guess field in the 3DMQ process, poor representation of the downslope winds that were occurring at this time. Including the HWAS observations in the analysis scheme at 09 UTC increased wind speeds by 4 m/s over most of the HWAS locations with a maximum increase of greater than 6.5 m/s in the vicinity of the Stadium and Community Center sensors as shown in the cross section in Figure 16.
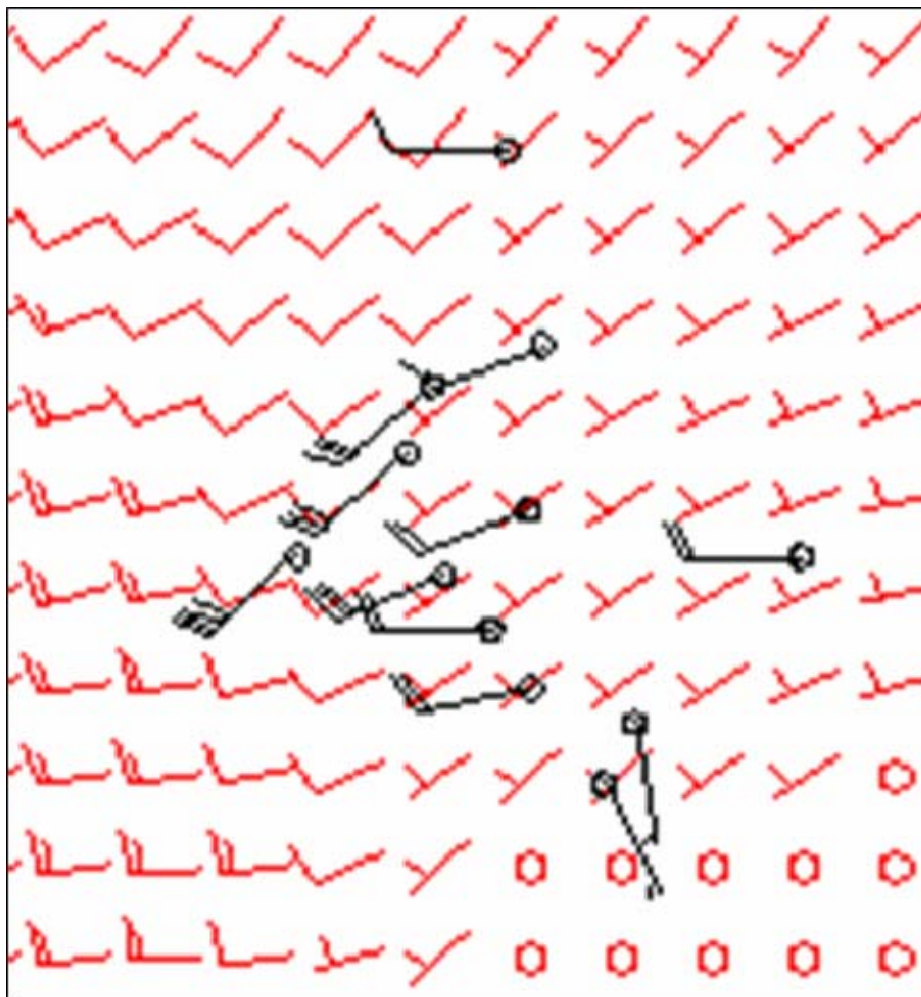
Figure 15.   Horizontal depiction of 1.33 km grids locations and spacing in relation to the HWAS sensor's locations. HWAS sensor's locations are represented by the circle at the base of the wind barb, and grid points are located at the base of the wind barbs without circles. Wind field is from the 09 UTC 6 March 2004 1.33 km analysis without HWAS observations included in the 3DMQ routine.
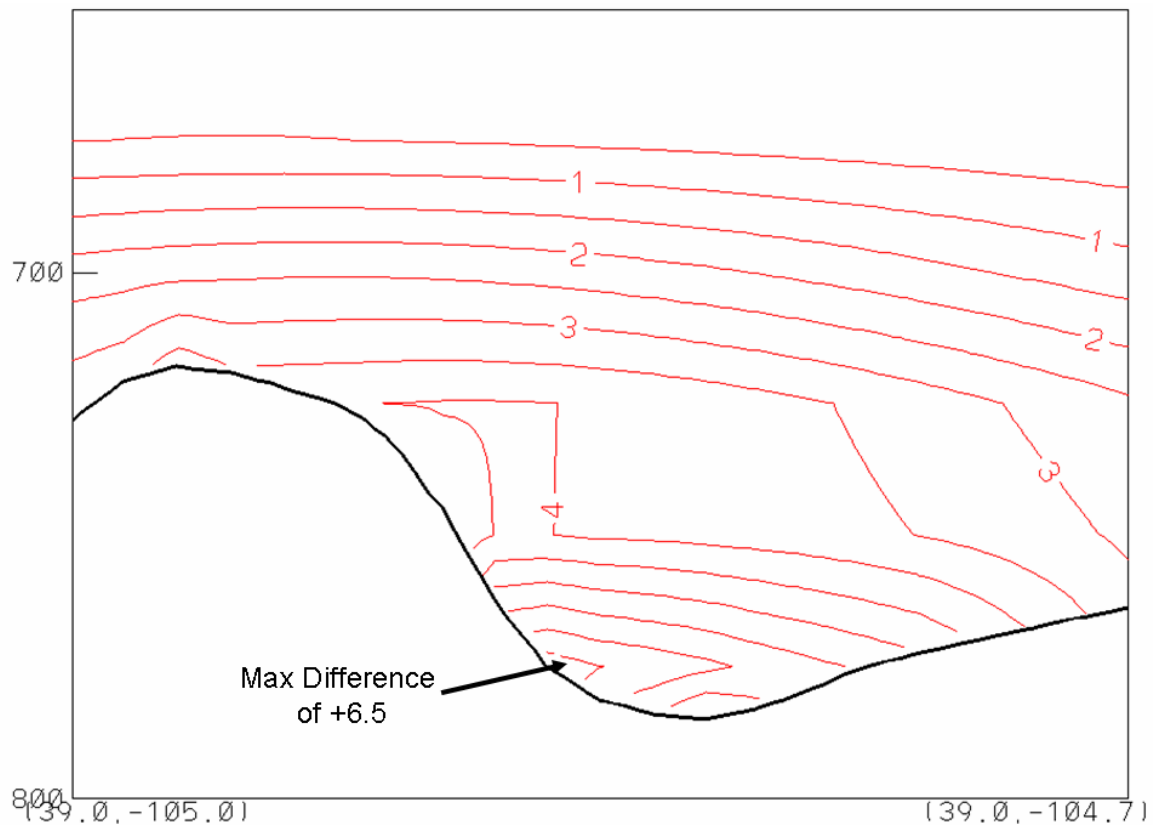
Figure 16.　　　Cross section from 09 UTC 6 March 2004 looking north along USAFA and Rampart Range depicting difference field for wind speed in m/s between 3DMQ analyses with HWAS observations included and without. Vertical axis is in mb.

51

SENSOR	1.33 km	4 km	12 km	AVERAGE
Aardvark	2.6926	2.3674	2.4209	2.4937
Airfield	2.8762	2.4737	2.9825	2.7774
Command Post	7.3769	7.0002	6.3804	6.9192
Community Center	8.0862	7.5150	6.8986	7.5000
Lewis Palmer	1.9557	2.0305	2.1348	2.0403
North Ridge	5.8513	5.6359	5.4554	5.6476
Pine Creek	4.6817	4.2722	4.1108	4.3549
Pine Valley	3.8217	3.4869	3.4778	3.5955
Rampart	14.1167	14.6429	13.6704	14.1433
South Gate	2.1463	2.0950	2.5998	2.2804
South Ridge	4.0775	3.6545	3.7231	3.8184
Stadium	3.0593	2.9623	3.2025	3.0747
AVERAGE	5.0618	4.8447	4.7548	

Table 5.   RMSE by sensor and grid resolution for wind speeds at HWAS observations locations for 3DMQ analyses performed hourly without HWAS observations included from 00 UTC 6 March through 00 UTC 7 March 2004. Wind speeds used to perform calculations are in m/s.

Table 5 depicts RMSE statistics generated from all HWAS locations by sensor and grid size from 00 UTC on 6 March through 00 UTC on 7 March 2004 during the high wind event at USAFA. The wind speed data from the HWAS observations were not included in the analyses done for the RMSE statistics shown in Table 5. Similarly to the RMSE values when verified by hour, Table 5 shows that the 1.33 km grids verified the worst, while the 12 km verified the best when verified by sensor. Also, likewise to the RMSE by sensor when HWAS observations were included in the analysis, the average RMSE when verified by sensor without the HWAS data included showed that sensors at higher elevations generally verified worse than sensors at lower elevations. The exception again is Lewis Palmer which had the best overall average RMSE of all sensors of 2.0403. In addition, Lewis Palmer along with the Airfield, Stadium, and South Gate locations were the only locations that verified better at 1.33 km than at 12 km when the HWAS observations were not included. This can be explained by the presence of other observations such as the CDOT sensors close to Lewis Palmer on I-25 and the METAR observation from KAFF (the

USAFA airfield runway sensor) that were included in the analyses through the MADIS dataset even if the HWAS data was left out.

Community Center - No HWAS

Figure 17.　　Graph of hourly steady state wind observations for the Community Center sensor versus 1.33 and 12 km analyzed values without HWAS observations included for 00 UTC 6 March through 00 UTC Mar 2004.

The poor performance of the 1.33 km grid when not including the HWAS observations in the analysis process suggests that increasing the resolution of an analysis without adding more observations will not lead to a more accurate analysis. A grid point in the larger 12 km domain essentially represents the mean of the smaller 1.33 km domain. A 12 km grid point along the western edge of the HWAS network would likely have stronger winds due to the higher terrain and thus transfer these higher winds to sensors in lower elevations during the verification process due to the coarser grid. Since the trend throughout most of the analyses was the underestimation of wind speeds by all size domains, this transference of the higher winds from a grid point in elevated terrain to the analyzed values at sensors in lower terrain could explain the lower RMSE for the

12 and 4 km analyses versus the 1 km analyses. When leaving the HWAS observations out of the analyses, the few MADIS or other METAR observations that are still included within the boundaries of the 1.33 km domain could also produce bad analyses causing the 12 km analyses to perform better than the more detailed but possibly out of phase 1.33 km analyses. In this study, a more accurate analysis could only be obtained when information from mesoscale observations were incl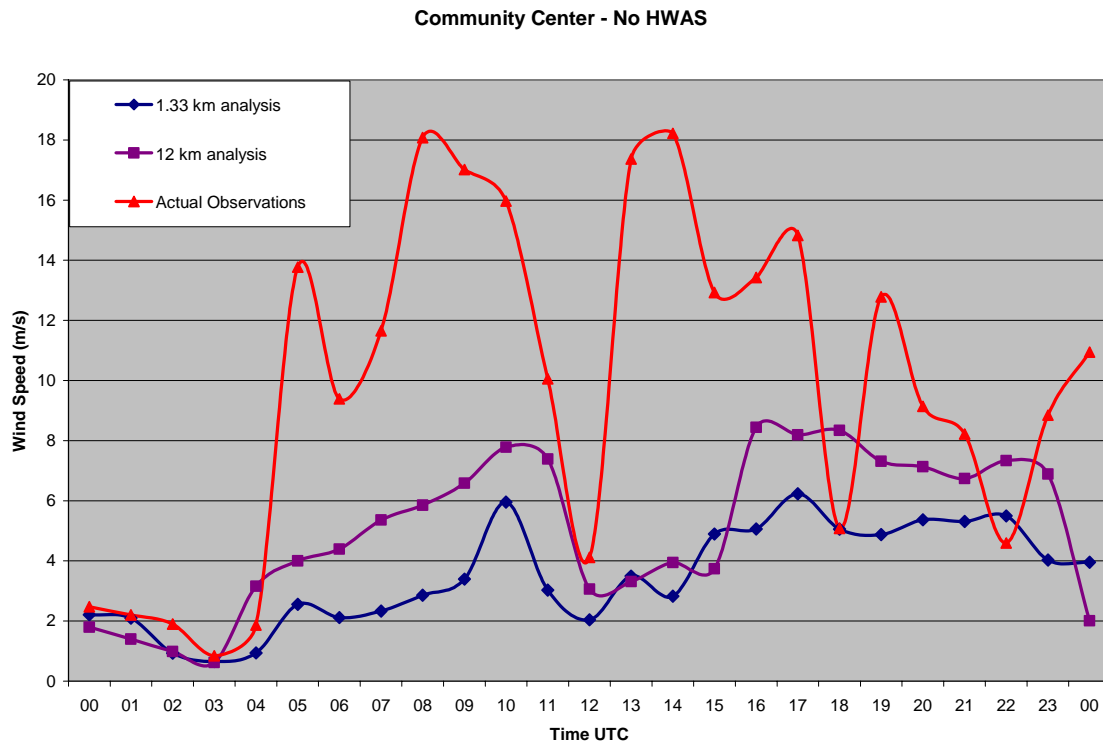uded along with a decrease in grid spacing. Figure 17 shows the hourly graph of actual steady state wind observations for the Community Center sensor versus 1.33 and 12 km analyzed values without HWAS observations included. This graph illustrates the inability of the 1.33 km analyzed grid to perform better than the 12 km grid when the HWAS observations are not included and again points to the deficiencies in the ETA model's first guess at accurately forecasting the intensity of the windstorm and hour this shortfall dominates the error in the analyzed fields created by 3DMQ.

B.   MM5 MODEL FORECASTS

Six model runs were created for this study. A triply-nested (12, 4, 1.33 km) MM5 model was run for 18 UTC on 5 March and 00 UTC and 06 UTC on 6 March 2004 with forecasts out 30, 24, and 18 hours respectively with all model runs ending at 00 UTC on 7 March 2004. Each of the three models runs were performed twice, once with analyses that included HWAS observations as part of the initial conditions and once with initial conditions without HWAS observations included. RMSE statistics were calculated for each hour of the model forecasts and compared to the analyses discussed in the previous section and to each other to determine the impact of the HWAS observations on the model forecasted winds and the overall depiction of the downslope windstorm by the different model runs. As with the analyses, RMSE verification statistics were generated at the HWAS locations only and nowhere else on the forecast grids were verified. This was performed to provide consistent measurement of performance over the area of interest around USAFA. Model forecast fields were

54

generated at one hour intervals for the 1.33 and 4 km grids, and at three hour intervals for the 12 km grids.

The overall average RMSE for wind speed from all 30 forecast hours from the 18 UTC 6 March 2004 MM5 model run indicate that the 1.33km forecast grid verified better at the HWAS locations than the 4 km forecast grid. These results are shown in Table 6 in tabular form and in Figure 18 in graphical form. The 1.33 km verified better with no discernable difference between when the HWAS observations were included in the initial conditions or when they were not. As shown in Figure 18, the 1.33 km grid had barely detectable differences between forecasts including the HWAS observations and those that did not for the first two hours of the model run and then the two model runs became virtually identical for the rest of the model run. This statement is also true for the 4 km grids, as there was no detectible difference between the two separate model runs beyond the two hour forecast. The RMSE averages shown in Table 6 for the later periods of the forecast run correspond to the forecast hours of the other model runs and are shown for comparison to those runs. The increase in the average RMSE across all model grids with time indicate that the 18 UTC model run did not capture important mesoscale or even synoptic scale features that caused the high winds late in the forecast period of these model runs.

FORECAST HOUR	ALL OBS		NO HWAS	
	1.33 km	4 km	1.33 km	4 km
040305/1800	0.6967	1.0341	0.8472	1.3151
040305/1900	1.3473	0.8620	1.7065	1.2442
040305/2000	0.9413	1.9376	0.9231	2.1101
040305/2100	1.4759	1.2558	1.4592	1.3265
040305/2200	1.9855	1.2702	2.0629	1.1789
040305/2300	1.4444	1.7273	1.4279	1.6573
040306/0000	2.1476	1.5560	2.1268	1.5571
040306/0100	2.0154	2.1219	1.9460	2.1321
040306/0200	1.0868	1.1781	1.0834	1.1824
040306/0300	2.5307	3.3495	2.5025	3.3347
040306/0400	3.1222	3.4910	3.1308	3.5023
040306/0500	7.3343	6.0985	7.3563	6.1275
040306/0600	3.5998	5.8618	3.6221	5.8619
040306/0700	5.8147	6.5762	5.3037	6.5538
040306/0800	9.3631	8.3267	9.3508	8.3305
040306/0900	7.7542	7.5730	7.6996	7.5770
040306/1000	3.4920	4.0004	3.3731	4.0043
040306/1100	5.7252	4.6397	5.8126	4.5819
040306/1200	5.5182	3.7185	5.5156	3.7140
040306/1300	9.9600	9.4425	9.9706	9.4540
040306/1400	10.6230	9.9180	10.6145	9.9324
040306/1500	8.7746	10.4542	8.7815	10.4377
040306/1600	8.3024	7.9640	8.3046	7.9382
040306/1700	5.3775	3.3501	5.2270	3.3117
040306/1800	4.9445	7.5116	4.9874	7.5295
040306/1900	5.4511	6.2416	5.4621	6.2567
040306/2000	3.8818	5.4373	3.8804	5.4405
040306/2100	3.8996	5.7987	3.8935	5.7996
040306/2200	4.8707	7.8849	4.8942	7.8934
040306/2300	2.5710	4.1162	2.5702	4.1375
040307/0000	2.4374	2.0944	2.4773	2.0914
AVERAGE	4.4674	4.7352	4.4617	4.7585
AVERAGE 5/18-5/23 UTC	1.3152	1.3479	1.4045	1.4720
AVERAGE 6/00-7/00 UTC	5.2239	5.5482	5.1955	5.5473
AVERAGE 6/06-7/00 UTC	5.9137	6.3637	5.8811	6.3603

Table 6.   RMSE by forecast hour and grid resolution for wind speeds at HWAS observations locations for the MM5 18 UTC 30 hour forecast model runs with HWAS observations included in the analyses used as initial conditions and without. Wind speeds used to perform calculations are in m/s.

5 March 18 UTC Model RMSE by Forecast Hour

Figure 18.   Graph of hourly RMSE for wind speeds at HWAS observations
locations for the MM5 18 UTC 30 hour forecast model runs with
HWAS observations included in the analyses used as initial
conditions and without. Wind speeds used to perform calculations
are in m/s.

| | | ALL OBS | | | NO HWAS | |
FORECAST HOUR	1.33 km	4 km	12km	1.33 km	4 km	12km
040306/0000	0.6316	0.8884	1.1653	0.6714	0.6905	0.9693
040306/0100	2.9991	2.7298		3.3749	2.9736	
040306/0200	1.1605	1.5698		1.1475	1.4105	
040306/0300	3.7619	3.9329	4.7405	3.6953	3.6984	4.7741
040306/0400	3.5400	4.7584		3.4551	4.6940	
040306/0500	3.5150	4.7356		3.4380	4.6092	
040306/0600	4.4861	2.0499	5.5486	4.1491	2.1186	5.5664
040306/0700	3.9770	3.1487		4.2372	3.2311	
040306/0800	5.1353	8.6142		5.0744	8.5476	
040306/0900	4.9088	7.7506	7.2305	4.3793	7.5313	7.2431
040306/1000	5.1572	5.3157		5.3091	5.0452	
040306/1100	5.6223	5.7422		4.1178	5.8526	
040306/1200	5.4096	6.1230	5.9027	5.3592	6.1195	5.8738
040306/1300	8.6322	9.1554		8.6927	9.1440	
040306/1400	9.5837	8.0142		9.5678	8.0138	
040306/1500	6.4805	6.5053	5.5754	6.6301	6.5021	5.5452
040306/1600	7.0934	6.9345		7.0633	6.8770	
040306/1700	5.7292	4.1116		5.7379	4.0703	
040306/1800	5.6748	7.6946	9.8919	5.7438	7.7582	9.9060
040306/1900	4.4888	6.1132		4.4975	6.1587	
040306/2000	3.9776	5.5057		3.9806	5.5467	
040306/2100	4.3853	5.9189	6.3717	4.3845	5.9447	6.3851
040306/2200	4.2494	8.0405		4.2721	8.0756	
040306/2300	2.6754	3.9766		2.6248	4.0505	
040307/0000	2.1397	2.1503	2.8246	2.1204	2.1312	2.8011
AVERAGE	4.6166	5.2592	5.4724	4.5490	5.2318	5.4516
AVERAGE 06-00 UTC	5.2530	5.9403	6.1922	5.1548	5.9326	6.1887

Table 7.   RMSE by forecast hour and grid resolution for wind speeds at HWAS observations locations for the MM5 00 UTC 24 hour forecast model runs with HWAS observations included in the analyses used as initial conditions and without. Wind speeds used to perform calculations are in m/s.
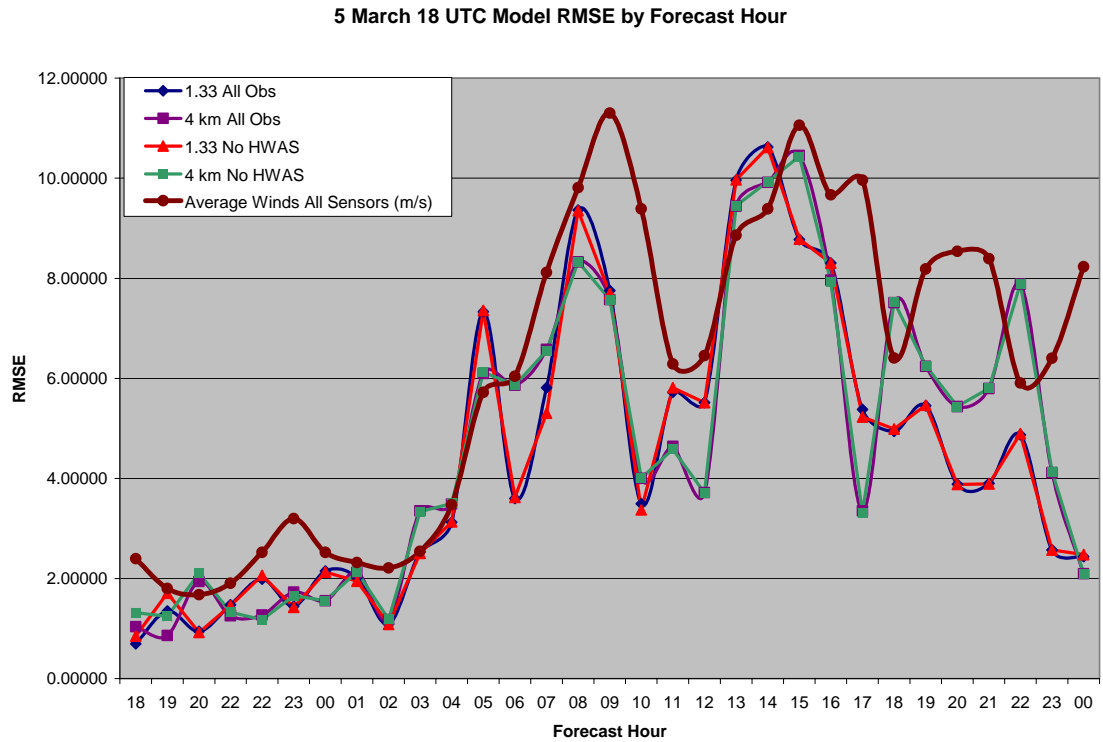
6 March 00 UTC Model RMSE by Forecast Hour
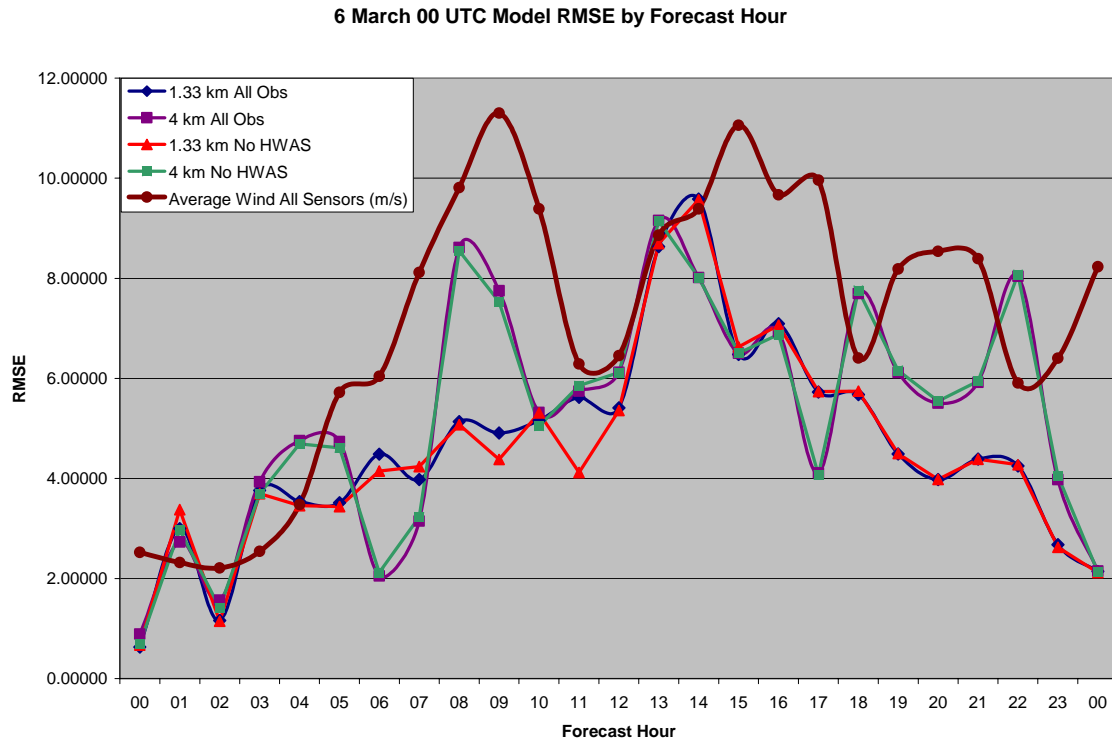
Figure 19.   Graph of hourly RMSE for wind speeds at HWAS observations locations for the MM5 00 UTC 24 hour forecast model runs with HWAS observations included in the analyses used as initial conditions and without. Wind speeds used to perform calculations are in m/s.

The 00 UTC MM5 model runs from 6 March performed better overall than the 18 UTC run and captured more of the structure and timing of the strong winds associated with this event. In particular, the 1.33 km forecast was much improved over the previous run in regard to the strength of the first wind maximum around 08-09 UTC as is shown by the lower RMSE for the 1.33 km grids during these hours in Figure 19. Again, as in the 18 UTC model run, the HWAS observations seemed to have little to no impact upon the overall average RMSE error for the 00 UTC runs. A small difference is observed in the RMSE by hour in the 1.33 km grids with and without HWAS through the first 12 hours of the 00 UTC model run, but then differences are almost indiscernible after that point. The 4 km forecasts were again almost completely identical over the entire period for this model run as they performed worse than the 1.33 km grid. The RMSE for

the 12 km forecast grids were calculated every three hours for the 00 UTC MM5 model runs and are displayed in Table 7. The 12 km three hour forecasts verified the worst of all grid domains in these model runs and for this reason and the fact that forecasts were only produced every three hours, the 12 km grids were not verified for any of the other model runs. It is assumed however, that similar results to those shown in Table 7 with respect to RMSE being greater than the 1.33 and 4 km forecast grids would be found in every model run during this event.

Rampart 00 UTC Model Output - HWAS Included
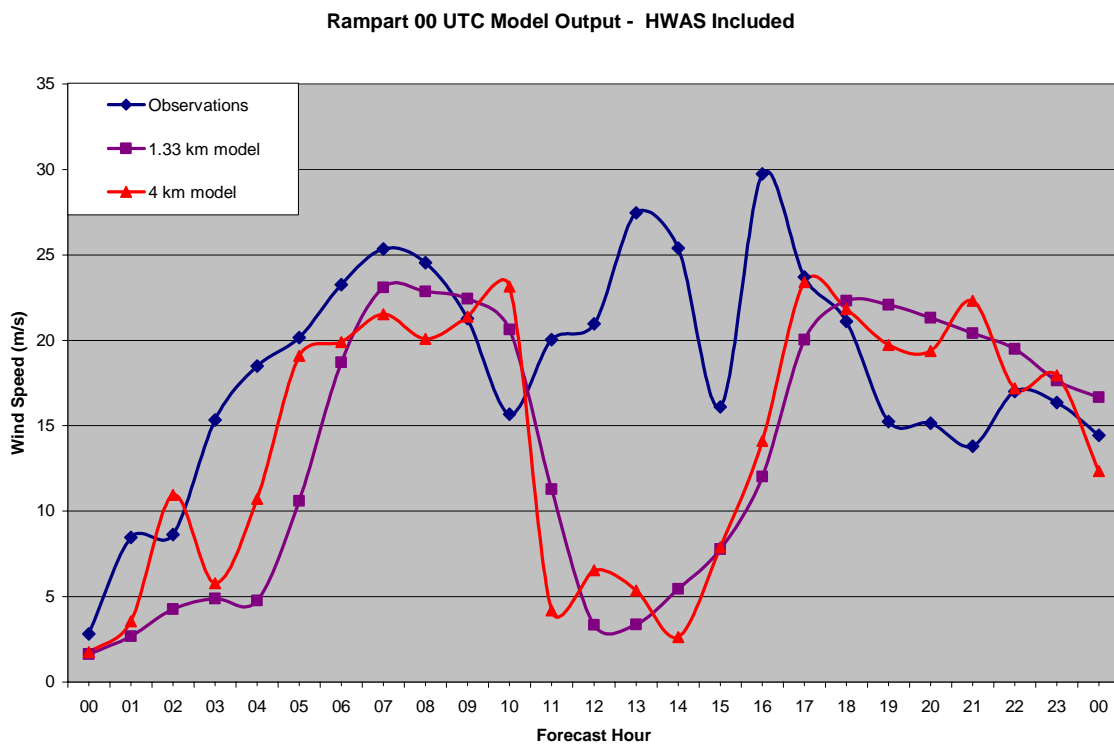
Figure 20.   Graph of hourly steady state wind observations for the Rampart sensor versus 1.33 and 4 km model forecast values with HWAS observations included in the initial analysis for the 00 UTC 24 hour forecast MM5 model run.
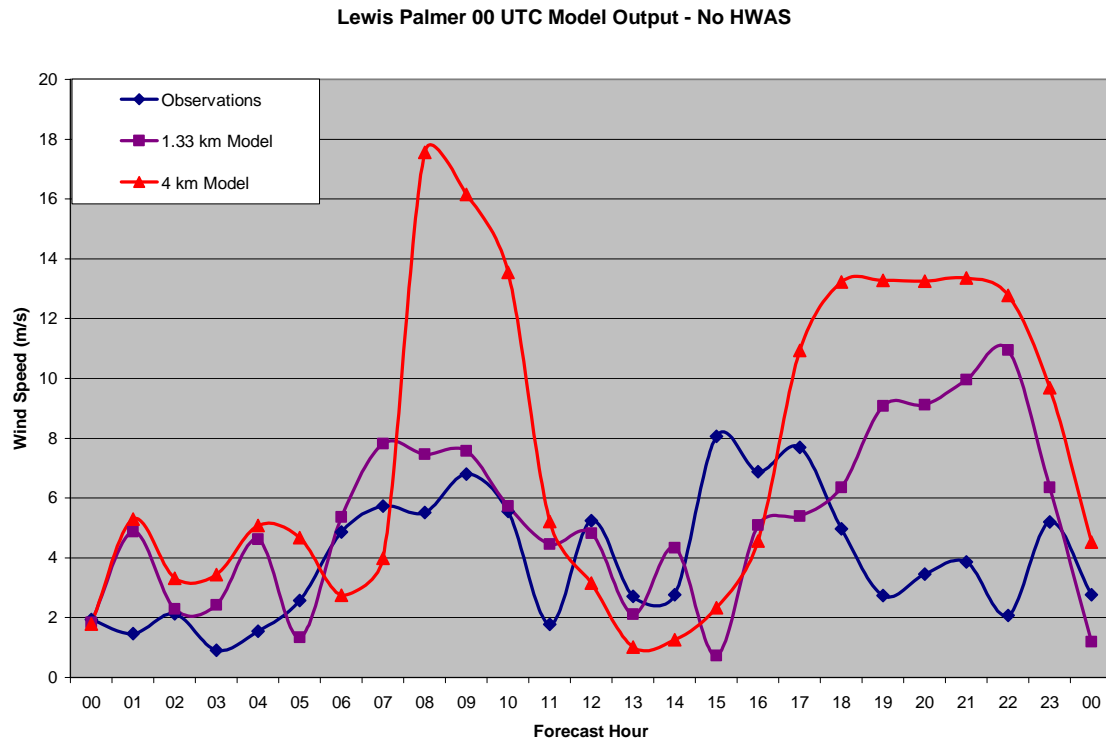
Figure 21.   Graph of hourly steady state wind observations for the Lewis Palmer sensor versus 1.33 and 4 km model forecast values without HWAS observations included in the initial analysis for the 00 UTC 6 24 hour forecast MM5 model run.

The 1.33 km grids verified particularly well for the first 12 hours of the 00 UTC model runs at almost all the HWAS sensors. This is illustrated in Figure 20 and Figure 21 where the 1.33 km forecast almost mirrored actual observations at both the Rampart and Lewis Palmer sensors. The Rampart sensor recorded the highest winds of all HWAS stations during this first wind maximum around 08-09 UTC, and both the 1.33 and 4 km forecasts did a good job at getting the timing and strength of this peak correct. However, at lower elevations the 4 km grid did a much poorer job forecasting wind speeds. This is clearly shown in Figure 21 where the 4 km forecasted wind speeds are almost 11 m/s above actual observed values at Lewis Palmer. The strong winds at Rampart, that continued during the lull at stations lower in elevation, were missed by both the 1.33 and 4 km forecasts, but both grid sizes did a fairly accurate job at timing the start of the

61

lull at other locations and is represented by the lower wind speeds and RMSE values at the Lewis Palmer sensor shown in Figure 21.

In the 00 UTC model run, both the 1.33 and 4 km forecast grids had a problem with the timing and intensity of the second wind maximum that occurred around 15 UTC. Most sensors above 2000 m had winds that increased rapidly between 13-14 UTC. Both the 1.33 and 4 km forecast grids failed to begin the second peak in winds until around 16-18 UTC causing the very high RMSE around 13-14 UTC as shown in Figure 19. The 1.33 and 4 km grids began to increase their winds around 16-18 UTC, but both models were sporadic at which sensors they verified well. This can be attributed to the high amount of forecast error late in the model run and the sharp temporal and spatial variations that downslope windstorms often produce across the varying topography. Two cross sections from the 00 UTC run are shown in Figure 22. They are taken from the 1.33 km model fields and show the models depiction of the second wind maximum as it progressed down the Rampart Range.
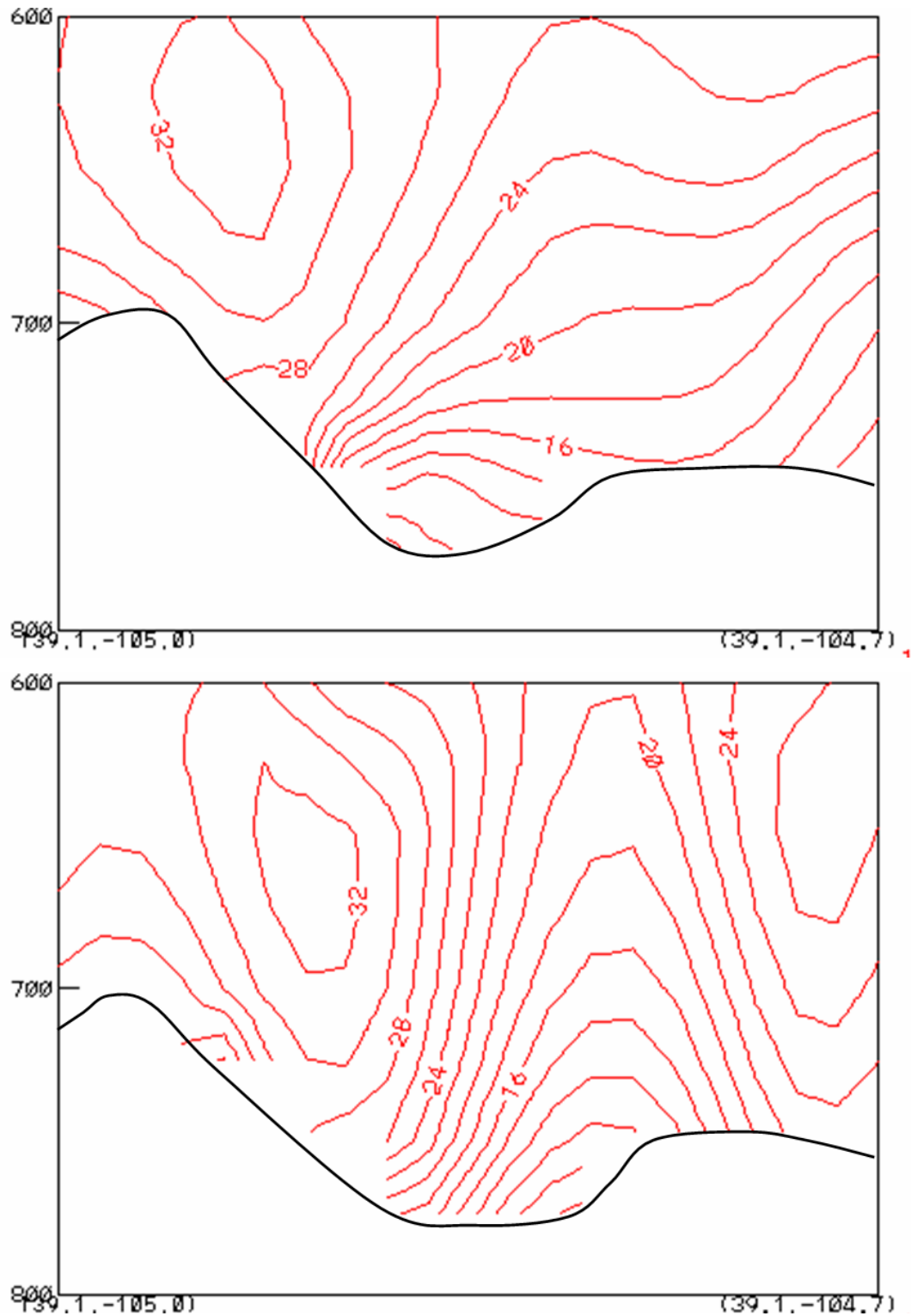
Figure 22.   Cross sections from the 1.33 km 00 UTC 6 March 2004 MM5
model run with all observations included looking north along
USAFA and Rampart Range depicting isotachs in m/s. The top plot
is the 16 hour forecast and the bottom plot is the 18 hour forecast.

The results from the 06 UTC 6 March 2004 MM5 model run were very similar to the same forecast hours in the 00 UTC model runs and are depicted in Table 8 and Figure 23. The 1.33 km forecast grids again performed better than the 4 km grids overall, however, the inclusion of the HWAS observations into initial analyses fields did create a discernable difference in the 1.33 km domain as shown in Table 8 and in Figure 23. Forecasts for the 1.33 km grid verified better with the HWAS observations than without on average across all locations five out of the first six hours of the model run. The start time of this particular model run was just prior to when the first peak of high winds occured and after the time when locations above the surface based inversion layer (2000 m and above) were already experiencing an increase in strong winds. Despite the influence of the HWAS observations early in this model run, no single location verified significantly better when averaged across the entire model run as depicted in Table 9. Additionally, when comparing 06-00 UTC forecast hours, the 00 UTC model runs verified better than the 06 UTC model runs over all. The 06 UTC model runs were plagued as earlier runs by an inability to properly forecast the timing and intensity variations of the second wind maximum late in the forecast period.

	ALL OBS		NO HWAS	
FORECAST HOUR	1.33 km	4 km	1.33 km	4 km
040306/0600	4.8017	5.7840	6.6245	6.5033
040306/0700	4.7219	7.4223	5.6729	7.4729
040306/0800	6.0772	7.6077	6.2082	7.6475
040306/0900	7.3493	5.8791	5.6627	6.1059
040306/1000	4.0645	5.5526	4.1427	5.3980
040306/1100	4.8630	7.6550	5.1157	7.8148
040306/1200	4.1930	4.6546	4.3087	4.5278
040306/1300	8.1590	8.5090	8.1581	8.5734
040306/1400	8.5849	7.5433	8.7272	7.5174
040306/1500	6.8478	6.1835	7.0168	6.1181
040306/1600	5.4698	6.6603	5.4912	6.7015
040306/1700	5.7053	4.8952	5.8589	4.7000
040306/1800	5.6739	5.9949	5.5554	5.8711
040306/1900	4.5563	4.6765	4.5404	4.6416
040306/2000	4.3288	4.1709	4.3226	4.1498
040306/2100	4.7676	4.1995	4.7729	4.1827
040306/2200	4.2976	6.6466	4.1990	6.5623
040306/2300	3.6971	3.6553	3.8370	3.5133
040307/0000	4.8812	2.1998	4.8319	2.1858
AVERAGE	5.4232	5.7837	5.5288	5.7993

Table 8.   RMSE by forecast hour and grid resolution for wind speeds at HWAS observations locations for the MM5 06 UTC 18 hour forecast model runs with HWAS observations included in the analyses used as initial conditions and without. Wind speeds used to perform calculations are in m/s.

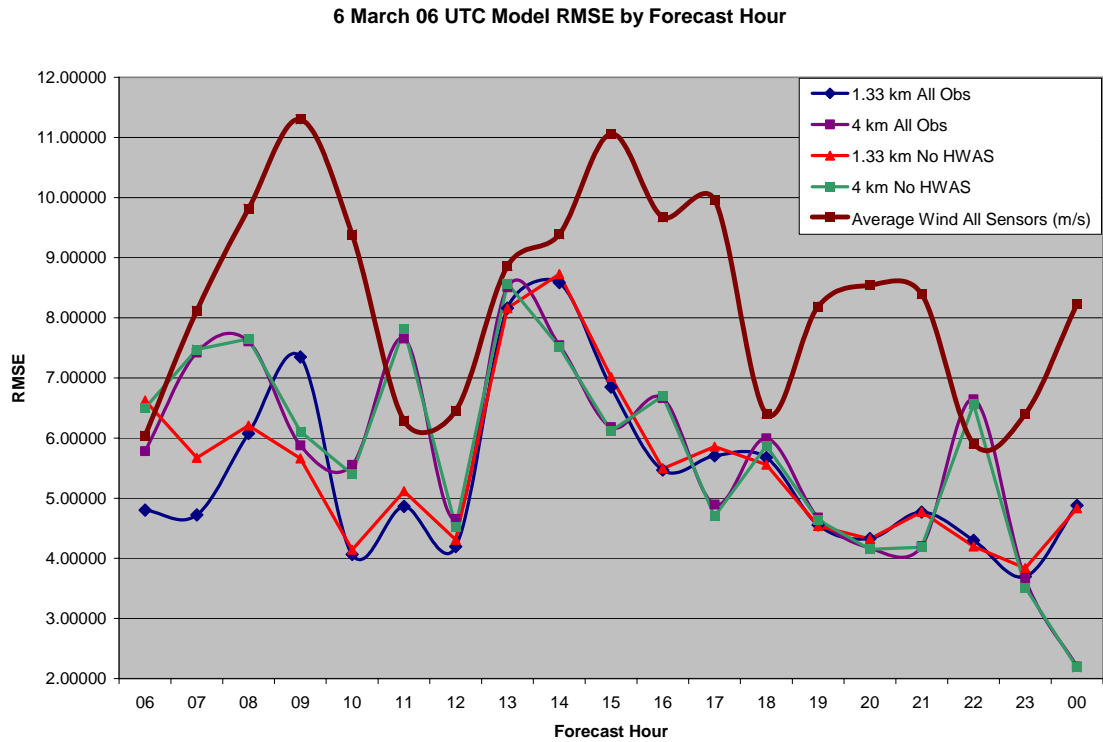**6 March 06 UTC Model RMSE by Forecast Hour**

Figure 23.   Graph of hourly RMSE for wind speeds at HWAS observations locations for the MM5 06 UTC 18 hour forecast model runs with HWAS observations included in the analyses used as initial conditions and without. Wind speeds used to perform calculations are in m/s.

06/00 UTC-24HR RUN	ALL OBS		NO HWAS	
SENSOR	1.33 km	4 km	1.33 km	4 km
Aardvark	2.4281	4.5916	2.4085	4.5536
Airfield	4.0130	3.0611	3.9218	3.0381
Command Post	6.6166	6.6770	6.5595	6.6685
Community Center	6.5738	6.1204	6.4778	6.1029
Lewis Palmer	3.4676	6.0554	3.4926	6.0057
North Ridge	5.4903	6.8470	5.4656	6.8538
Pine Creek	3.9207	4.0601	3.9594	4.1034
Pine Valley	3.5392	5.4807	3.6747	5.4068
Rampart	9.3370	9.7998	9.1134	9.7752
South Gate	3.2732	3.1574	3.1687	3.1566
South Ridge	4.0868	4.2254	3.9233	4.2041
Stadium	3.1423	5.2463	3.1519	5.1931
AVERAGE	4.6574	5.4435	4.6098	5.4218

Table 9.   RMSE by HWAS sensor and grid resolution for wind speeds at HWAS observations locations for the MM5 18 UTC 30 hour forecast model runs with HWAS observations included in the analyses used as initial conditions and without for all model forecast hours. Wind speeds used to perform calculations are in m/s.

THIS PAGE INTENTIONALLY LEFT BLANK

V. CONCLUSIONS AND FUTURE WORK

A. CONCLUSIONS

This study evaluated the data assimilation capabilities of 3DMQ and the MM5 model when incorporating mesoscale observations from the USAFA HWAS observation network. A severe downslope wind event from 6 March 2004 at USAFA was selected for study to test both the analysis capabilities of 3DMQ and forecast accuracy of the MM5 when HWAS observations were included in initial analysis fields and when they were left out. Difference fields and RMSE verification statistics were generated for these cases to compare the 3DMQ analyses and MM5's forecast ability for winds at USAFA.

This study shows that incorporating HWAS observations into the 3DMQ data assimilation process has a significant impact upon verification of analyzed wind fields, with the biggest impact occurring at the 1.33 km grid scale. The 1.33 km analyzed wind fields verified better than any of the other gird sizes when the HWAS observations were included at every hour analyzed in this study. Additionally, the 4 km gird verified better than the 12 km at all but a few hours when the HWAS observations were included. When the HWAS observations were left out of the analyzed wind fields, the exact opposite findings were true, with the 12 km grid verifying the best and the 1.33 km verifying the worst. These findings give evidence to the critical importance of including mesoscale observations when performing a mesoscale analysis. A reasonable inference from these results suggest that increasing the resolution of an analysis alone will not lead to more accurate representations of the atmosphere. It is only when more data is included in the analysis that a more truthful analysis can occur in regions of complex terrain. While these conclusions were arrived at by only analyzing one strong downslope wind event, it is reasonable to assume that in areas of complex terrain where rapid temporal and spatial changes of weather often occur similar results will be found in future case studies.

Using the analyzed fields produced by the 3DMQ data assimilation process as initial conditions for MM5 model simulations, this study shows the ability of the 1.33 km model forecast wind fields to verify significantly better than either the 4 or 12 km through 18, 24, and 30 hour forecasts. Consistently during the model simulations performed in this study, the MM5 verified better whether the HWAS observations were included or not on the higher resolution grids out to 30 hours. These results show that the MM5 when given a detailed enough terrain representation and fine resolution nested grid structure with sufficient size to capture both synoptic and local conditions has the ability to forecast winds in complex terrain better at the 1-2 km scale than at courser resolutions. This finding is significant as many previous studies had only found that at such high resolutions the resultant forecasts were more realistic, but they did not necessarily verify better when compared to forecasts from courser resolutions. These results give promise to the ability of NWP models to accurately forecast not only wind speeds at such fine resolution, but also other meteorological variables.

This study shows the limited, yet discernable impact HWAS observations have upon forecasted winds in the first several hours of MM5 model runs during a severe downslope wind event at USAFA. Only one of the three model simulations performed in this study showed significant difference between forecasts with HWAS observations included in the analyses used as initial conditions and those without. This result shows the time sensitive nature of forecast model runs and suggests the need for rapid updates of new real time information into the data assimilation process of NWP models. Also, this result suggests that model runs can show significant changes when given new data over just a few hours. Lastly, it should be noted that the HWAS sensors are not necessarily placed at locations to best sample the atmosphere and capture the mesoscale structure. Most of these sensors are placed at areas that are either operationally significant (i.e. Command Post, Community Center, Airfield) or sited in a location due to access roads, schools, or demographic reasons (i.e. Lewis Palmer, Pine Creek, Pine Valley). The addition of more sensors or moving

current sensors to areas that are more favorable to capturing the mesoscale structure of weather features would likely enhance the ability to produce more accurate analyses and model forecasts. The largest impact may be produced if more sensors were added along the ridgeline atop the Rampart Range in positions that would complement the Rampart sensor which is currently the only sensor at this elevation.

B.   FUTURE WORK

Due to the promising results shown by this study and continued data collection of weather events by the HWAS network, there are many aspects of this research that would be worthy of future investigation. The time intensive nature of NWP model simulations and large amount of data produced for analysis by the MM5 model limited this study to examine only one particular strong downslope wind event. The unique positioning of the HWAS observations in an area of complex terrain make them an ideal data set for use in continued research into the effects of mountains on the weather they help to produce and the ability of forecaster to accurately analyze and model these weather events. Future work can continue research on not only high wind events, but also into the plethora of other weather phenomena common at USAFA and recorded by the HWAS sensors. Listed below are several areas of research where future work would provide additional insight to the problems and results presented in this study.

1. Using the methods of this study, examine other case studies where strong downslope wind events were recorded by the HWAS sensors. Strong downslope winds can be caused by many different synoptic patterns and have different dynamic signatures (i.e. chinook versus bora). These different cases may provide additional insight to the ability of the HWAS network to capture the necessary data to properly analyze and forecast these events. The

examination of other wind events is essential to the validation or refutation to the findings of this study.

2. Determine the impact of HWAS observations on other areas of the grid (i.e. downstream effects). This will help determine the impact of placing tactical observations in areas upstream or around a battlespace and the effect upon analyses and NWP forecasts.

3. Adjust the weights given to observations in the data assimilation process. Also, perform NWP model runs with the domains larger/smaller and with different orientations than the domains in this study. This will help determine the optimum domain size and orientation for NWP models run on this scale when attempting to incorporate mesoscale observations into analyses and forecasts.

4. Examine the importance of the other sources of data for this study with the idea of simulating the data sparsity or data denial for regions of military operations. Networks such as MADIS do not exist in many other nations, and the incorporation of such data along with HWAS observations does not accurately reflect the density of data readily available for model simulations in areas where the military often operates. If the other data sources such as MADIS, RAOB's, METAR's, etc. were denied, the effect of adding a mesoscale network such as HWAS to analyses and model forecasts could be greatly different than the results found in this study.

5. Find other data that can help simulate information available in the military battlespace and evaluate the effect of this data in concert with HWAS observations in forecasts and analyses. Potential sources for such data could be affixing sensors to any of the many different aircraft that fly at USAFA in support of the aviation training that occurs there. Gathering data from a glider, tow plane, Unmanned Aerial Vehicle (UAV) or other aircraft could simulate the

ability of the military to fly a UAV or even a manned aircraft over a battlespace and incorporate the weather information recorded by these aircraft into mesoscale analyses and NWP models for use in planning and real time support of military operations.

6. Evaluate variables other than wind for verification within analyses and model forecasts. This could help understand the ability of NWP models to predict these variables on the resolutions used in this study.

Each of these proposed future areas of work will greatly add to a better understanding of the importance of where and what kind of data is needed to properly forecast at finer resolutions for a targeted battlespace used in military operations. Through studies like the one presented in this thesis and future work proposed to follow this study, it will be possible to incorporate all battlefield data into relocatable NWP model simulations that can provide critical weather information to the planners and operators for military operations on the scale of 1-2 km in the near future.

THIS PAGE INTENTIONALLY LEFT BLANK

LIST OF REFERENCES

Aanenson, C. J. M., 1965: Gales in Yorkshire in February 1962. Geophys. Mem., **14,** 1-44.

Arakawa, S., 1969: Climatological and dynamical studies on the local strong winds, mainly in Hokkaido, Japan. Deophys. Mag., **34,** 359-425.

Astling, E. G., and Coauthors, 1985: Boundary Layer Control of Nocturnal Convection Associated with a Synoptic Scale System. Monthly Weather Review, **113,** 540-552.

Berri, G. J., and J. Paegle, 1989: Sensitivity of Local Predictions to Initial Conditions. Journal of Applied Meteorology, **29,** 256-257.

Brinkman, W.A.R, 1974: Strong downslope winds at Boulder, Colorado. Monthly Weather Review, **102,** 592-602.

Clark, T. L., and W. R. Peltier, 1977: On the evolution and stability of finite amplitude mountain waves. J. Atmos. Sci., **34,** 1715-1730.

Colle, B. A., and C. F. Mass, 1998: Windstorms along the Western Side of theWashington Cascade Mountains. Part I: A high-resolution observational and modeling study of the 12 February 1995 event. Monthly Weather Review, **126,** 28-52.

Cunningham, Jeffery G., 2007: Personal Communication.

Descloitres, J., MODIS Land Rapid Response Team, cited March 2007. [Available online at http://www.14ers.com/images/ranges3db700x414.jpg.]

Durran, D.R., 1986: Another look at downslope winds. Part I: The development of analogs to supercritical flow in an infinitely deep, continuously stratified fluid. J. Atmos. Sci., **43,** 2527-2543.

Durran, D. R., and J. B. Klemp, 1987: Another look at downslope winds. Part II: Nonlinear amplification beneath wave-overturning layers. J. Atmos. Sci., **22,** 3402-3412.

Hart, K. A., W. J. Steenburgh, and D. J. Onton, 2005: Model Forecast Improvements with Decreased Horizontal Grid Spacing over Finescale Intermountain Orography during the 2002 Olympic Winter Games. Weather and Forecasting, **20,** 558-576.

Houghton, D. D., and E. Isaacson, 1968: Mountain winds. Stud. Num. Anal., **2,** 21-52.

Klemp, J.B., and Lilly, D.R. 1975: The Dynamics of Wave-Induced Downslope Winds. Journal of the Atmospheric Sciences, **32**, 320–339.

Kuettner, J., 1959: The rotor flow in the lee of mountains. GRD Res. Notes No. 6, Geophys. Res. Directorate, Air Force Cambridge Res. Center.

Lorenz, E. N., 1963: Deterministic Nonperiodic Flow. Journal of the Atmospheric Sciences, **20,** 130-141.

Mass, C. F., D. Ovens, K. Westrick, and B. A. Colle, 2002: Does increasing horizontal resolution produce more skillful forecasts? The results of two years of real-time numerical weather prediction over the Pacific Northwest. Bulletin of the American Meteorological Society, **83,** 407-430.

McQueen, J. T., R. R. Draxler, and G. D. Rolph, 1995: Influence of Grid Size and Terrain Resolution on Wind Field Predictions from an Operational Mesoscale Model. Journal of Applied Meteorology, **34,** 2166-2181.

NCEP, cited March 2007: Product Document Description. [Available online at http://www.nco.ncep.noaa.gov/pmb/nwprod/analysis/PDDwebsite_200403.txt.]

Nuss, W. A. and D. W. Titley, 1994: Use of Multiquadratic Interpolation for Meteorological Objective Analysis. Monthly Weather Review, **122,** 1611-1631.

Nuss, W. A., 2007: Personal Communication.

Oard, Michael J.. 1993: A Method for Predicting Chinook Winds East of the Montana Rockies. Weather and Forecasting, **8,** 166–180.

Onton, D. J., and W. J. Steenburgh, 2001: Diagnostic and Sensitivity Studies of the 7 December 1998 Great Salt Lake-effect snowstorm. Monthly Weather Review, **129,** 1318-1328.

Paegle, J., 1984: Topographically bound low-level circulations. Riv. Meteor. Aeronaut., **44,** 113–125.

Paegle, J., and Coauthors, 1990: Predictability of Flows Over Complex Terrain, Meteorology Monograph No 45, American Meteorological Society, 285-299.

Paegle, J., and T. Vukicevic, 1987: On the predictability of low-level flow during ALPEX. Meteorology and Atmospheric Physics, **36**, 45-60.

Schultz, David M., and Coauthors, 2002: Understanding Utah Winter Storms: The Intermountain Precipitation Experiment. Bulletin of the American Meteorological Society, **83,** 189-210.

Scorer, R.S., and H. Klieforth, 1959: Theory of mountain waves of large amplitude. Quart. J. Roy. Meteor. Soc., **85,** 131-143.

Shuman, Frederick G., 1989: History of Numerical Weather Prediction at the National Meteorological Center. Weather and Forecasting, **4**, 286-296.

Smith, R., and Coauthors, 1997: Local and Remote Effects of Mountains on Weather: Research Needs and Opportunities. Bulletin of the American Meteorological Society, **78**, 877-892.

Smith, R. B., 1977: The steepening of hydrostatic mountain waves. J. Atmos. Sci., **34,** 1634-1654.

UCAR, cited March 2007: ETA Introduction. [Available online at http://www.meted.ucar.edu/nwp/pcu2/etintro.htm.]

UCAR, cited March 2007: NAM Model Changes. [Available online at http://www.meted.ucar.edu/nwp/pcu2/NAMWRFjun2006.htm.]

UCAR, cited March 2007: Operational Models Matrix. [Available online at http://www.meted.ucar.edu/nwp/pcu2/.]

UCAR, cited March 2007: GFS Introduction. [Available online at http://www.meted.ucar.edu/nwp/pcu2/avintro.htm.]

UCAR, cited March 2007: MM5 Community Model. [Available online at http://www.mmm.ucar.edu/mm5/.]

Vukicevic, T. and J. Paegle, 1989: The Influence of One-Way Interacting Lateral Boundary Conditions upon Predictability of Flow in Bounded Numerical Models. Monthly Weather Review, **117,** 340-350.

THIS PAGE INTENTIONALLY LEFT BLANK

INITIAL DISTRIBUTION LIST

1. Defense Technical Information Center
   Ft. Belvoir, VA

2. Dudley Knox Library
   Naval Postgraduate School
   Monterey, CA

3. 25th Operational Weather Squadron
   Davis Monthan AFB, AZ

4. Meteorology Program
   USAFA, CO

5. XPF and DNX
   Air Force Weather Agency
   Offut AFB, NE